

Research Paper

# Multi-cohort validation of a lipid metabolism and ferroptosis-associated index for prognosis and immunotherapy response prediction in hormone receptor-positive breast cancer

Cheng Zeng<sup>1\*</sup>, Jiani Wang<sup>1\*</sup>, Shen Zhao<sup>2</sup>, Yuhan Wei<sup>1</sup>, Yalong Qi<sup>1</sup>, Shuning Liu<sup>1</sup>, Yuanyi Wang<sup>1</sup>, Hewei Ge<sup>1</sup>, Xiaoqi Yang<sup>3</sup>, Yujing Tan<sup>1</sup>, Yizhou Jiang<sup>2✉</sup>, Haili Qian<sup>3✉</sup>, Fei Ma<sup>1✉</sup>

1. Department of Medical Oncology, National Cancer Center/National Clinical Research Center for Cancer/Cancer Hospital, Chinese Academy of Medical Sciences and Peking Union Medical College, Beijing, 100021, China.
2. Key Laboratory of Breast Cancer in Shanghai, Department of Breast Surgery, Fudan University Shanghai Cancer Center, Shanghai Medical College, Fudan University, Shanghai 200032, China; Department of Oncology, Shanghai Medical College, Fudan University, Shanghai, 200032, China.
3. State Key Laboratory of Molecular Oncology, National Cancer Center/National Clinical Research Center for Cancer/Cancer Hospital, Chinese Academy of Medical Sciences and Peking Union Medical College, Beijing, 100021, China.

\*These authors have contributed equally to this work.

✉ Corresponding authors: Yizhou Jiang, email: yizhoujiang@fudan.edu.cn; Haili Qian, email: qianhaili@pumc.edu.cn; Fei Ma, email: mafei@cicams.ac.cn. ORCID: Cheng Zeng, <https://orcid.org/0000-0002-9392-8259>; Fei Ma, <https://orcid.org/0000-0001-9432-1902>.

© The author(s). This is an open access article distributed under the terms of the Creative Commons Attribution License (<https://creativecommons.org/licenses/by/4.0/>). See <https://ivyspring.com/terms> for full terms and conditions.

Received: 2025.03.04; Accepted: 2025.05.18; Published: 2025.06.09

## Abstract

**Background:** Hormone receptor-positive (HR+) breast cancer exhibits significant heterogeneity influenced by lipid metabolism and ferroptosis (LMF). While immune checkpoint inhibitors have shown promise in neoadjuvant therapy, as evidenced by the KEYNOTE-756 and CheckMate 7FL trials, identifying the optimal patient population remains challenging. This study aims to classify molecular clusters based on LMF-related genes and develop the LMF\_index to predict prognosis and immunotherapy response in HR+ breast cancer.

**Methods:** Transcriptome and clinical data of HR+ breast cancer were obtained from the Cancer Genome Atlas and Gene Expression Omnibus databases. Unsupervised clustering based on prognostic LMF-related genes identified molecular clusters, followed by tumor mutational burden (TMB) and immune microenvironment (TME) analysis. The LMF\_index was constructed using least absolute shrinkage and selection operator and multivariate Cox regression analyses and validated across multiple internal and external cohorts. Its predictive value for neoadjuvant immunotherapy efficacy was assessed using GSE173839. Validation at the transcriptomic level was conducted in the Shanghai cohort, while protein-level validation was performed using multiplex immunohistochemistry (mIHC) on a tissue microarray comprising 113 breast cancer samples. Spatial analyses further examined the distribution of key panel genes within the TME.

**Results:** Two molecular clusters were identified in this study. Cluster 1 exhibited higher TMB, tumor purity, and Ki-67, while Cluster 2 showed greater CD8+ T cells and elevated PD-1, PD-L1, and CTLA4 expression. The LMF\_index, derived from a seven-gene panel (KRT5, CD209, KLRB1, MRC1, UGT2B4, FABP7, and BIRC3), effectively stratified patients into high and low LMF\_index groups, with high LMF\_index patients showing significantly shorter overall survival. Patients with a low LMF\_index demonstrated elevated ACSL4 expression, enhanced immune activity, higher immunophenoscores, and increased pathological complete response rates following neoadjuvant immunotherapy, indicating a greater potential benefit from immunotherapy. The prognostic value of the LMF\_index was validated at the transcriptomic level in the Shanghai cohort and at the protein level using mIHC on a tissue microarray. Spatial analysis further demonstrated KLRB1 enrichment in the tumor stroma, correlating with CD8+ T cell and M1 macrophage infiltration, and an enhanced response to immunotherapy.

**Conclusions:** This study identified distinct LMF-related molecular clusters in HR+ breast cancer with unique prognostic and immune characteristics. The LMF\_index shows potential as a prognostic biomarker and a guide for immunotherapy strategies in HR+ breast cancer.

Keywords: lipid metabolism, ferroptosis, immunotherapy, ACSL4, hormone receptor-positive breast cancer

## 1. Introduction

Breast cancer is one of the most common malignancies worldwide. According to the global cancer statistics report, approximately 2.3 million new breast cancer cases were diagnosed in 2022, accounting for 11.6% of all cancers, making it the second most common cancer[1]. Breast cancer is primarily classified based on the expression of estrogen receptor (ER), progesterone receptor (PR), and human epidermal growth factor receptor 2 (HER2), into subtypes including hormone receptor-positive (HR+) breast cancer, HER2+ breast cancer, and triple-negative breast cancer (TNBC)[2, 3]. HR+ breast cancer is the most common subtype, accounting for 70% of all breast cancer cases[3]. Current standard treatment for HR+ breast cancer primarily relies on endocrine therapy, including selective estrogen receptor modulators (SERMs), aromatase inhibitors (AIs), and selective estrogen receptor degraders (SERDs)[4, 5]. In recent years, the addition of cyclin-dependent kinase 4/6 (CDK4/6) inhibitors to endocrine regimens has significantly improved progression-free survival (PFS) and overall survival (OS) in patients with advanced HR+ breast cancer[6-9]. Moreover, targeted therapies such as PI3K inhibitors and mTOR inhibitors are available for selected patients harboring PIK3CA mutations[10, 11]. Despite these advances, therapeutic resistance remains a major challenge, and most patients with advanced HR+ breast cancer eventually experience disease progression[12, 13]. Furthermore, not all patients are eligible for targeted therapies due to the absence of actionable genetic alterations, limiting the effectiveness of precision oncology in this population.

Given these therapeutic limitations, immunotherapy has emerged as a promising approach in HR+ breast cancer. Immune checkpoint inhibitors (ICIs), such as those targeting PD-1, PD-L1, or CTLA-4, have shown remarkable success in several cancer types by reactivating cytotoxic T cells to eliminate tumor cells[14, 15]. However, HR+ breast cancer is generally characterized by a "cold" immune phenotype with low tumor-infiltrating lymphocytes and limited PD-L1 expression, contributing to the relatively poor responsiveness to ICIs observed in this subtype[16, 17]. Nevertheless, recent clinical trials have provided new insights into the potential of ICIs in HR+ breast cancer. The phase III KEYNOTE-756 and CheckMate 7FL studies demonstrated that combining ICIs with neoadjuvant chemotherapy significantly improved the pathological complete response (pCR) rate in ER+/HER2- breast cancer patients[18, 19]. However, the observed increase in pCR was only approximately 10%, highlighting the

limited overall benefit of ICIs in this subtype. The lack of reliable predictive biomarkers poses a significant challenge in optimizing patient selection and maximizing therapeutic outcomes. Since the efficacy of ICIs is closely linked to the tumor microenvironment (TME), a comprehensive characterization of the immune landscape and the development of robust biomarkers are essential for stratifying HR+ breast cancer patients. Identifying the subset most likely to benefit from ICIs will enhance the precision and efficacy of immunotherapy in this population.

Lipid metabolism plays a crucial role in the initiation and progression of tumors[20, 21]. Lipid metabolic processes such as fatty acid synthesis, oxidation, and cholesterol metabolism are closely linked to the development of breast cancer, and disturbances in lipid metabolism are associated with immune escape and drug resistance[22-24]. Ferroptosis, a distinct form of programmed cell death, is tightly linked to lipid metabolism, with fatty acid accumulation inducing oxidative stress and triggering cell death[25]. Conversely, the occurrence of ferroptosis may alter the metabolic state of tumor cells, influencing lipid metabolism processes[26]. Moreover, recent studies suggest that ferroptosis can influence immune cell recruitment and function within the TME, potentially impacting the effectiveness of immunotherapies[27]. Given the close interplay among lipid metabolism, ferroptosis, and immune regulation, we hypothesized that an integrative analysis of genes associated with lipid metabolism and ferroptosis (LMF) may yield a more robust framework for characterizing the immune landscape and identifying molecular clusters in HR+ breast cancer. In recent years, some researchers have utilized either lipid metabolism or ferroptosis-related genes to evaluate tumor prognosis and predict immunotherapy response[28-31]. However, their combined impact in HR+ breast cancer has not been systematically elucidated. Therefore, integrating LMF-related genes into a unified analytical model may deepen our understanding of the TME, and enhance the development of personalized immunotherapeutic strategies.

In this study, we combined LMF-related genes for unsupervised clustering analysis, classifying HR+ breast cancer patients into two molecular clusters. We then constructed and validated the LMF\_index across multiple cohorts to evaluate the prognosis of HR+ breast cancer patients. Furthermore, we explored the potential value of the LMF\_index in reflecting TME features and predicting the efficacy of immunotherapy. Lastly, we validated the prognostic ability of the LMF\_index using the Shanghai cohort

and multiplex immunohistochemistry (mIHC) on breast cancer tissue microarrays. Further analysis revealed that high expression of KLRB1 is associated with increased infiltration of CD8+ T cells and M1 macrophages, as well as an improved response to

immunotherapy. These findings offer new insights into prognosis prediction and immunotherapy for HR+ breast cancer. The study design is depicted in **Figure 1**.

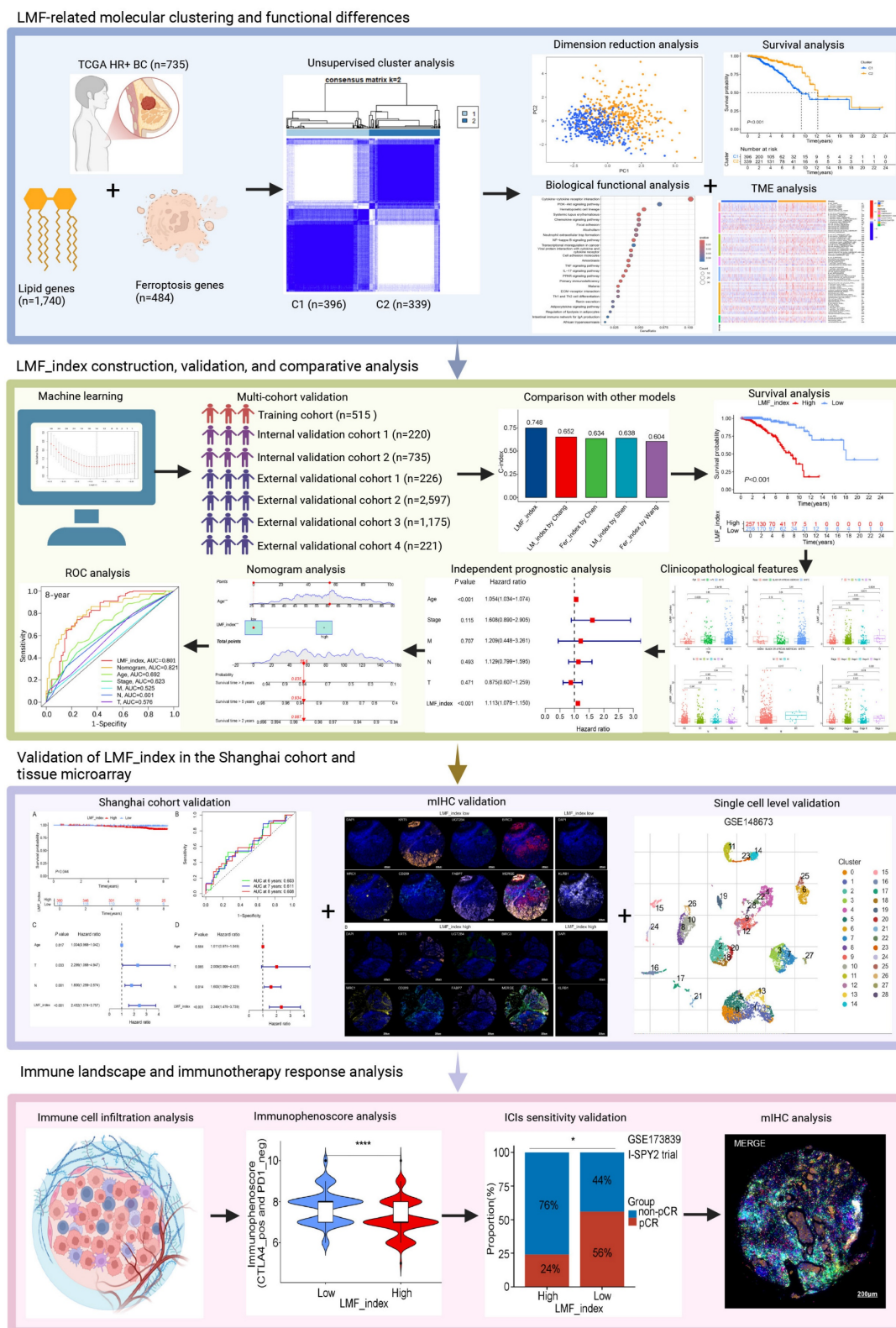


Figure 1. Flowchart of the study design.

## 2. Materials and Methods

### 2.1. Data collection and preprocessing

Transcriptomic data and corresponding clinical information for the Cancer Genome Atlas-breast invasive carcinoma (TCGA-BRCA) cohort were downloaded from the TCGA GDC database (<https://portal.gdc.cancer.gov/>) in January 2024. The dataset initially contained 1,097 breast cancer tissue samples. After excluding 105 samples with OS of less than 30 days or missing survival status, 241 TNBC and HER2+ samples, and 16 samples with incomplete clinical staging, 735 HR+ breast cancer samples were included in this study. Among them, 485 patients had documented records of receiving endocrine therapy. HR+ breast cancer was defined as ER and/or PR expression greater than 1% by immunohistochemistry. The 735 HR+ samples were randomly divided into a training cohort (n=515) and internal validation cohort 1 (n=220) using a 7:3 split with seed-based random assignment[32]. The GSE159956 dataset includes 295 breast cancer samples, of which 226 were HR+ samples. The GSE7390 dataset includes 198 breast cancer samples, with 134 HR+ samples. To increase the sample size for external validation, the gene expression matrices of 226 HR+ samples from GSE159956 and 134 HR+ samples from GSE7390 were batch-corrected and merged using the combat algorithm to form external validation cohort 1 using the sva package (version 3.54.0)[33]. The GSE96058 dataset contains 3,069 breast cancer samples. After removing 100 duplicate samples and 372 TNBC and HER2+ samples, 2,597 HR+ samples were included as external validation cohort 2. Among these, 2,141 patients had documented records of receiving endocrine therapy. Transcriptomic data and clinical information for the METABRIC dataset were downloaded from the cBioPortal database (<https://www.cbioportal.org/>) in January 2024. The METABRIC dataset includes 2,509 breast cancer samples, of which 528 were excluded due to missing survival time or status, and 806 TNBC or HER2+ samples were also removed, leaving 1,175 HR+ samples for external validation cohort 3. Among these, 856 patients had documented records of receiving endocrine therapy. The GSE173839 dataset contains 50 HR+ breast cancer patients who received neoadjuvant immunotherapy. A total of 484 ferroptosis-related genes were obtained from the FerrDb database (<http://www.zhounan.org/ferrdb/current/>) in December 2023 (Table S1). A total of 1,740 lipid metabolism-related genes used in this study were obtained from our previously published work (Table S2)[34].

### 2.2. Unsupervised clustering analysis of LMF-related genes

In this study, differential expression analysis of LMF-related genes between HR+ breast cancer and normal tissues was performed using the limma package (version 3.62.1)[35]. The selection criteria for differential expression genes (DEGs) were set at  $|\log_2FC| > 1$  with an adjusted  $P$ -value  $< 0.05$ [36]. Next, a univariate Cox regression analysis was conducted on these DEGs to assess their prognostic value. Genes with a  $P$ -value  $< 0.01$  were selected for unsupervised clustering analysis using the ConsensusClusterPlus package (version 1.70.0)[37]. The consensus cumulative distribution function (CDF) under various cluster numbers was used to evaluate cluster stability and determine the optimal number of clusters. Principal component analysis (PCA) and t-distributed stochastic neighbor embedding (t-SNE) were employed to visualize the distribution characteristics of the different clusters[38]. OS and disease-free survival (DFS) of patients between two clusters were analyzed based on survival time and status.

### 2.3. Biological functional analysis between LMF-related molecular clusters

To investigate the biological functional differences between molecular clusters classified based on LMF-related genes, we first assessed the tumor mutational burden (TMB) and the overall mutational landscape between the two clusters. DEGs between the molecular clusters were identified using the limma package (version 3.62.1), with the threshold set at  $|\log_2FC| > 1$  and an adjusted  $P$ -value  $< 0.05$ [35, 36]. Functional enrichment analyses, including Gene Ontology (GO) enrichment analysis and Kyoto Encyclopedia of Genes and Genomes (KEGG) pathway analysis, were performed to elucidate the biological processes and pathways associated with these DEGs. To evaluate differences in the TME, the ESTIMATE algorithm was applied to compare stromal scores, immune scores, and overall ESTIMATE scores between the molecular clusters[39]. Furthermore, key immune checkpoint molecules, including PD-1, PD-L1, and CTLA4, as well as estrogen receptor alpha (ER $\alpha$ ), Ki67, and components of the PI3K/AKT/mTOR signaling pathway, were analyzed to assess their expression differences across the clusters. A comprehensive assessment of immune cell infiltration was conducted using multiple computational algorithms, including TIMER, CIBERSORT, CIBERSORT-ABS, QUANTISEQ, MCPcounter, xCell, and EPIC, ensuring a robust characterization of immune landscape variations between the clusters[40, 41]. In addition, hematoxylin

and eosin (H&E) staining was performed on HR+ breast cancer tissue samples to analyze lymphocyte infiltration levels[42], further validating the computational immune profiling results.

#### 2.4. Construction of a prognostic LMF\_index and comparison with existing indices

To construct a prognostic LMF\_index and evaluate its predictive performance, we first conducted univariate Cox regression analysis on the DEGs between the two molecular clusters. To minimize overfitting, prognosis-related genes identified from the univariate analysis were further subjected to least absolute shrinkage and selection operator (LASSO) regression analysis using the glmnet package (version 4.1.8)[43]. The optimal  $\lambda$  value was determined via 10-fold cross-validation to achieve the best predictive performance for LMF-related genes[32, 36]. Subsequently, multivariate Cox regression analysis was performed to refine the LMF-related gene panel and determine their corresponding regression coefficients. An LMF\_index was then calculated based on the selected genes using the following formula[36, 38, 44]:

$$\text{LMF\_index} = \sum_{i=1}^n \beta_i * \text{expression level of gene}_i$$

The relationships among LMF\_index groups, molecular clusters, and survival outcomes were illustrated using Sankey diagrams. To assess the prognostic value of the LMF\_index, we compared its predictive performance with existing indices, including the ferroptosis-related index by Wang *et al.*[28], the ferroptosis-related index by Chen *et al.*[29], the lipid metabolism-related index by Chang *et al.*[30], and the lipid metabolism-related index by Shen *et al.*[31]. To ensure consistency with the literature, gene expression levels corresponding to each index were extracted, and multivariate Cox regression analysis was applied to obtain the respective regression coefficients for each gene[45]. The indices for each patient were then calculated. The predictive performance and clinical utility of the LMF\_index were evaluated using concordance index (C-index), receiver operating characteristic (ROC) curve analysis, and survival analyses, providing a comprehensive comparison with previously established prognostic indices[45].

#### 2.5. Internal and external validation of the LMF\_index

The performance of the LMF\_index was first assessed in the training cohort, while two internal validation cohorts (internal validation 1 and internal validation 2) were employed for internal validation of

the LMF\_index. To increase the sample size for external validation, we merged the GSE159956 and GSE7390 datasets after batch effect correction to form external validation 1. In addition, external validation 2 (GSE96058), external validation 3 (METABRIC dataset), and external validation 4 (Kaplan-Meier Plotter) were used for independent external validation of the LMF\_index. First, a scatter plot was generated in the training cohort to visualize the relationship between the LMF\_index and survival status of HR+ breast cancer patients. Kaplan-Meier survival analysis was then conducted to compare OS between LMF\_index low and LMF\_index high groups. Furthermore, ROC curves were plotted to evaluate the sensitivity and specificity of the LMF\_index for predicting 2-year, 5-year, and 8-year survival rates in patients with HR+ breast cancer. The same analyses were performed in the two internal validation cohorts and the three external validation cohorts. In external validation 4 (Kaplan-Meier Plotter), OS and recurrence-free survival (RFS) were analyzed in ER-positive breast cancer patients.

#### 2.6. Clinical subgroup survival analysis based on the LMF\_index

To further evaluate the performance of the LMF\_index across different clinical subgroups, we conducted Kaplan-Meier survival analysis stratified by clinicopathological characteristics of HR+ breast cancer patients. The subgroups analyzed included age ( $\leq 40$  years, 40-70 years,  $\geq 70$  years), race (White, Asian, Black or African American), tumor stage (T1, T2, T3, T4), nodal status (N0, N1, N2, N3), metastatic status (M0, M1), and overall disease stage (Stage I, Stage II, Stage III, Stage IV).

#### 2.7. Independent prognostic analysis and nomogram construction for the LMF\_index

To investigate prognostic factors in HR+ breast cancer patients, both univariate and multivariate Cox regression analyses were performed, incorporating clinicopathological characteristics and the LMF\_index. Additionally, a nomogram combining clinicopathological characteristics and the LMF\_index was constructed to predict patient prognosis[38]. The predictive accuracy of the nomogram was evaluated using the C-index. Furthermore, ROC curve analysis was performed to assess the predictive performance of the nomogram score, LMF\_index, and clinical factors (age, overall disease stage, T stage, N stage, M stage) for 2-year, 5-year, and 8-year survival outcomes in HR+ breast cancer patients[32].

## 2.8. Association between the LMF\_index and the TME landscape

To explore the TME landscape in HR+ breast cancer, multiple algorithms, including XCELL, TIMER, QUANTISEQ, MCPOUNTER, CIBERSORT-ABS, and CIBERSORT, were utilized to assess the spearman correlation between the LMF\_index and the levels of immune cell infiltration, and bubble plots were generated to visualize these relationships[40, 41]. Subsequently, the ESTIMATE algorithm was applied to analyze the stromal score, immune score, and total ESTIMATE score for LMF\_index high and LMF\_index low groups[39]. Additionally, the CIBERSORT method and single-sample gene set enrichment analysis (ssGSEA) were conducted to evaluate differences in immune cell infiltration levels and the activity of immune-related pathways between different LMF\_index populations[46, 47].

## 2.9. Evaluation of immunotherapy sensitivity based on the LMF\_index

To evaluate the clinical relevance of the LMF\_index in predicting ICIs response, spearman correlation analysis was first conducted to assess its association with immune checkpoint-related gene expression. Then, immunophenoscores (IPS) for TCGA-HR\_BRCA patients were obtained from the Cancer Immunome Atlas (TCIA) (<http://tcia.at/>). IPS was compared between the LMF\_index high and LMF\_index low groups, with higher IPS indicating greater sensitivity to ICIs[32, 36]. To validate the predictive value of the LMF\_index in immunotherapy response, data from the GSE173839 dataset (I-SPY2 clinical trial) were analyzed. Pathological complete response (pCR) rates were compared between LMF\_index high and LMF\_index low groups following neoadjuvant immunotherapy.

## 2.10. Analysis of expression levels of LMF\_index panel genes

To assess the expression patterns of LMF\_index panel genes in normal breast tissue and breast cancer tissue, we utilized data from the University of Alabama at Birmingham Cancer data analysis portal (UALCAN) (<https://ualcan.path.uab.edu/analysis.html>). Additionally, to explore the expression profiles of LMF\_index panel genes at the single-cell level, we employed the Tumor Immune Single-cell Hub 2 (TISCH2) (<http://tisch.comp-genomics.org/home/>), a comprehensive single-cell RNA sequencing (scRNA-seq) database focusing on the TME. Specifically, the GSE148673 dataset was used to analyze the LMF\_index panel genes from a single-cell

perspective, providing insights into its expression levels in tumor cells and immune cells.

## 2.11. Patients and tissue samples

The tissue microarrays used in this study, which consisted of tumor samples from 136 breast cancer patients, were procured from Shanghai Outdo Biotech Company in full compliance with the relevant regulations. The study was conducted in accordance with the ethical principles outlined in the Declaration of Helsinki. Written informed consent was obtained from all participants, ensuring voluntary participation. The use of human tumor tissue samples was approved by the Ethics Committee of Shanghai Outdo Biotech Company (approval number: YBM-05-01, YBM-05-02).

## 2.12. Multiplex immunohistochemistry staining and image acquisition

The mIHC staining protocol was validated by the EACRI IHC Core at the Providence Cancer Institute (Portland, OR), and the methods have been previously reported[48]. This study utilized consecutive sections from a tissue microarray. One section was stained for KRT5, UGT2B4, BIRC3, MRC1, CD209, and FABP7, while the other section was stained for PanCK, CD8, KLRB1, PD-L1, CD68, and CD163. An additional section was stained for PanCK, CD8, ACSL4, and GPX4 to evaluate the spatial distribution of ferroptosis-related proteins and immune cell infiltration within the epithelial and stromal compartments. Briefly, the tissue microarray slides were baked at 63°C for 1 hour, followed by deparaffinization using a fully automatic staining machine (LEICAST5020, LEICA). Antigen retrieval was performed after deparaffinization. Endogenous peroxidase activity was quenched using commercial hydrogen peroxide for 10 minutes. The microarrays were blocked for 10 minutes before being incubated for 1 hour with one of the following primary antibodies to perform mIHC staining: anti-CD68 (dilution: 1:500, Abcam), anti-CD8 (dilution: 1:500, Abcam), anti-CD163 (dilution: 1:300, Abcam), anti-PD-L1 (dilution: 1:200, Abcam), anti-PanCK (dilution: 1:200, Abcam), anti-KLRB1 (dilution: 1:50, Abcam), anti-KRT5 (dilution: 1:1000, Proteintech), anti-MRC1 (dilution: 1:200, Abcam), anti-FABP7 (dilution: 1:50, Abcam), anti-BIRC3 (dilution: 1:400, Abcam), anti-UGT2B4 (dilution: 1:50, Abcam), anti-CD209 (dilution: 1:50, Abcam), anti-ACSL4 (dilution: 1:100, Abcam), and anti-GPX4 (dilution: 1:100, Abcam). After washing the slides with TBST buffer, secondary antibody incubation was carried out using ready-to-use secondary antibodies (SM802, DAKO) for 10 minutes. Subsequently, Opal dye (Opal

7-color Manual IHC Kit, NEL801001KT, PerkinElmer) was applied and incubated at room temperature for 10 minutes. Microwave treatment was employed to remove the antibody complex between each cycle of staining. These steps were repeated until all markers in the panel were stained. Slides were counterstained with DAPI for 5 minutes and mounted using antifade mounting medium.

Multispectral imaging of the slides was conducted using the Tissue-FAXS system (TissueFAXS Spectra, TissueGnostics GmbH, Vienna, Austria). The acquired image data were imported into Strata-Quest analysis software (version 7.1.129, TissueGnostics GmbH, Vienna, Austria) for further processing. Spectral unmixing was performed to separate single-channel fluorescence signals, with the DAPI channel utilized for nuclear identification. A distance radius was defined based on the staining patterns of each protein channel, with the nucleus serving as a reference, enabling the detection of specific protein fluorescence signals. Thresholds were set according to the staining patterns of each channel, allowing for the identification and quantification of positively stained cell populations. The number and intensity of cells exhibiting single, double, or multiple positive staining were recorded for subsequent analysis.

### 2.13. Statistical analysis

Statistical analyses were performed using R software (version 4.3.0) and GraphPad Prism (version 8.2.1). Differences between categories were assessed using the Wilcoxon test for continuous variables and the Chi-square test for categorical variables. OS was compared across various categories using Kaplan-Meier curves, with statistical significance evaluated via the log-rank test. To identify independent prognostic factors, univariate and multivariate Cox regression analyses were performed. The predictive ability of the LMF\_index was assessed using ROC curves and nomograms. For comparisons between two groups, continuous variables were analyzed using the t-test (for normally distributed data) or the Mann-Whitney U test (for non-normally distributed data). A  $P$ -value of  $<0.05$  was considered statistically significant. The following significance thresholds were used:  $*P < 0.05$ ;  $**P < 0.01$ ;  $***P < 0.001$ ;  $****P < 0.0001$ .

## 3. Results

### 3.1. Molecular clustering based on LMF-related genes in HR+ breast cancer

In this study, we identified 422 DEGs associated with LMF (Figure S1A and Table S3). Univariate Cox

regression analysis further revealed 13 DEGs significantly associated with prognosis in HR+ breast cancer ( $P < 0.01$ , Figure S1B). Correlation heatmap analysis and protein-protein interaction (PPI) network demonstrated strong associations among TNFSF4, TP63, CD24, ESR1, and PRLR, suggesting their potential roles in HR+ breast cancer progression (Figure S1C-D). To classify molecular clusters, we performed unsupervised clustering analysis, stratifying patients into two distinct molecular clusters: cluster 1 ( $n=396$ ) and cluster 2 ( $n=339$ ) (Figure 2A and Figure S2A). PCA and tSNE demonstrated a clear separation between cluster 1 and cluster 2, confirming the robustness and stability of the molecular classification derived from ConsensusClusterPlus analysis (Figure 2B and Figure S2B). Kaplan-Meier survival analysis revealed that patients in cluster 2 exhibited significantly longer OS and DFS compared to those in cluster 1 (both  $P < 0.001$ , Figure 2C and Figure S2C). Furthermore, a heatmap of gene expression profiles highlighted significant differences in expression patterns between the two molecular clusters (Figure 2D). In summary, these findings demonstrate that HR+ breast cancer can be classified into two distinct molecular clusters based on LMF-related gene expression, with cluster 2 exhibiting a more favourable prognosis compared to cluster 1.

### 3.2. Biological functional differences between the two LMF-related molecular clusters

To elucidate the biological mechanisms underlying the prognostic differences between the two molecular clusters, we first assessed TMB levels in cluster 1 and cluster 2. The results demonstrated that patients in cluster 1 exhibited significantly higher TMB compared to those in cluster 2 (Figure S3A). Mutation analysis revealed that genes such as CDH1, MYH9, and UBR5 displayed higher mutation frequencies in cluster 1, whereas GATA3, CSMD2, and TG exhibited higher mutation rates in cluster 2 (Figure S3B). To further explore the functional differences between the two molecular clusters, differential gene expression analysis identified 1,102 DEGs (adjusted  $P < 0.05$ , Table S4). GO enrichment analysis revealed that these DEGs were significantly involved in production of molecular mediators of immune response, T cell receptor complex, receptor-ligand activity, and cytokine activity (Figure S3C). KEGG pathway analysis showed enrichment in cytokine-cytokine receptor interaction, PI3K-AKT signaling pathway, and NF-kappa B signaling pathway (Figure S3D), suggesting potential differences in the immune microenvironment between the two molecular clusters.

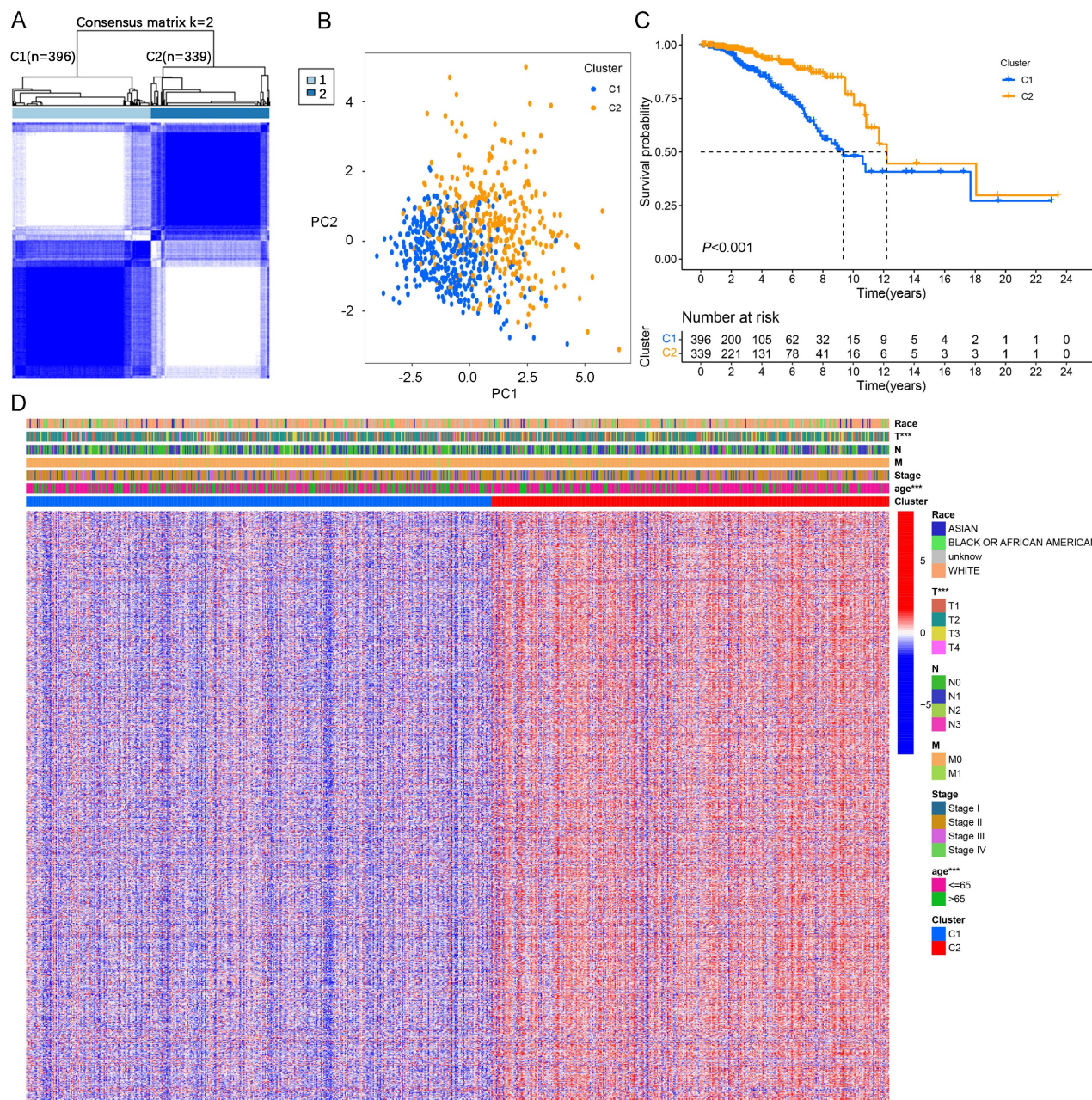


**Figure 2. Molecular clusters of LMF-related genes in HR+ breast cancer. (A)** Consensus matrix of unsupervised clustering analysis. **(B)** Principal Component Analysis (PCA) plots showing distinct separation between the two identified molecular clusters. **(C)** Kaplan-Meier survival curves comparing overall survival (OS) between the two molecular clusters. **(D)** Heatmap illustrating gene expression profiles and clinicopathological characteristics across the two molecular clusters. \*\*\* $P < 0.001$ .

To further evaluate differences in TME composition, the ESTIMATE algorithm was applied to assess immune and stromal components based on gene expression data. The analysis demonstrated that patients in cluster 1 had significantly lower stromal score, immune score, and ESTIMATE score compared to those in cluster 2 (Figure 3A), indicating higher tumor purity in cluster 1 and greater immune cell infiltration in cluster 2. Additionally, immune checkpoint expression analysis revealed significantly higher expression levels of PD-1, PD-L1, and CTLA-4 in cluster 2 compared to cluster 1 (Figure 3B-D).

Moreover, patients in cluster 1 exhibited significantly higher expression of PI3K, AKT, mTOR, ER, and Ki-67 compared to those in cluster 2, suggesting more active proliferative signaling in cluster 1 (Figures S3E-I). To further characterize immune infiltration patterns, multiple methods were employed. A heatmap analysis demonstrated that cluster 2 tumors exhibited significantly higher immune cell infiltration than cluster 1 tumors (Figure 3E). This finding was corroborated by H&E staining, which showed increased lymphocyte infiltration in cluster 2 tumor tissues compared to cluster 1 (Figure 3F).

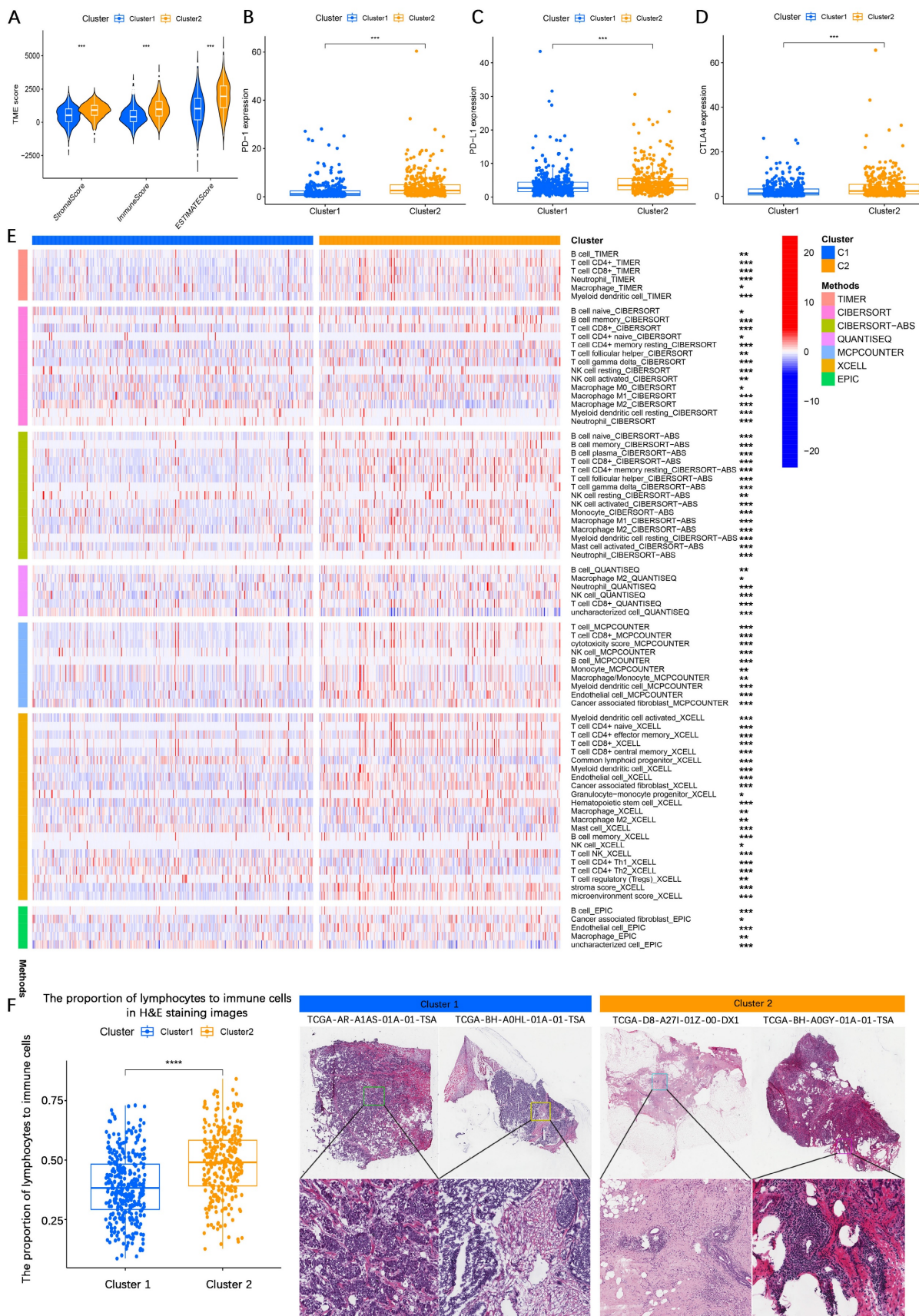


**Figure 3. Biological functional analysis of LMF-related molecular clusters in HR+ breast cancer. (A)** Analysis of stromal score, immune score, and ESTIMATE score between the two clusters using the ESTIMATE algorithm. The comparison indicates differences in the tumor microenvironment (TME) composition. **(B-D)** Differential expression analysis of immune checkpoint molecules PD-1, PD-L1, and CTLA4 between the two molecular clusters. The variation in expression suggests potential differences in immune evasion mechanisms and responses to immunotherapy. **(E)** Immune cell infiltration analysis comparing the two molecular clusters based on multiple algorithms, providing

a comprehensive overview of immune cell infiltration patterns. (F) Hematoxylin and eosin (H&E) staining comparison across different molecular clusters, indicating more lymphocytic infiltration in cluster 2. \* $P < 0.05$ ; \*\* $P < 0.01$ ; \*\*\* $P < 0.001$ ; \*\*\*\* $P < 0.0001$ .

Collectively, these findings suggest that HR+ breast cancer patients in cluster 1 exhibit higher tumor purity, more aggressive malignant characteristics, and lower immune infiltration, whereas patients in cluster 2 display greater immune cell infiltration and upregulated immune checkpoint expression, which may contribute to a relatively better prognosis.

### 3.3. Construction and validation of the LMF\_index and comparison with existing indices

Given the significant prognostic differences observed between the two molecular clusters based on LMF-related genes, we sought to develop a robust prognostic index (LMF\_index) for HR+ breast cancer. To achieve this, we conducted univariate Cox regression analysis on the 1,102 DEGs identified between the two clusters, leading to the selection of 55 genes significantly associated with prognosis (Table S5). To assess the robustness of the LMF\_index, the HR+ breast cancer cohort ( $n = 735$ ) was randomly divided into a training cohort ( $n = 515$ , Table S7) and a testing cohort ( $n = 220$ , Table S8) at a 7:3 ratio. The training cohort was used to construct the LMF\_index. Subsequently, LASSO regression analysis was performed to prevent overfitting, using the optimal  $\lambda$  value, which refined the gene panel to 14 genes (Figure S4A-B and Table S6). Further refinement through multivariate Cox regression analysis identified seven key genes: KRT5, CD209, KLRB1, MRC1, UGT2B4, FABP7, and BIRC3 (Figure 4A). The LMF\_index was then constructed based on the expression levels of these genes and their corresponding regression coefficients, formulated as follows:  $LMF\_index = (-0.23034 \times KRT5) + (0.66262 \times CD209) + (-0.63397 \times KLRB1) + (0.49821 \times MRC1) + (0.17847 \times UGT2B4) + (-0.33535 \times FABP7) + (-0.28564 \times BIRC3)$ . Patients were subsequently stratified into LMF\_index high and LMF\_index low groups based on the median LMF\_index. In the training cohort, a scatter plot of the risk index and survival status revealed that patients with a high LMF\_index had a higher death rate (Figure 4B). Further analysis revealed that patients with a high LMF\_index were predominantly from cluster 1, with significantly higher LMF\_index compared to those in cluster 2 (Figure 4C and Figure S4C). Kaplan-Meier survival analysis demonstrated significantly shorter OS in LMF\_index high patients compared to LMF\_index low patients ( $P < 0.001$ , Figure 4D). These findings were consistently replicated in both internal validation cohorts (internal validation cohorts 1 and

2) and external validation cohorts (external validation cohorts 1, 2, and 3), where LMF\_index high patients exhibited significantly worse OS outcomes (Figure 4E-I). In external validation cohort 4, LMF\_index high patients also demonstrated poorer recurrence-free survival (RFS) in addition to lower OS (Figure S4D).

To assess the predictive performance of the LMF\_index, we compared it with previously established indices, including ferroptosis\_index (Wang *et al.*, Chen *et al.*) and lipid metabolism\_index (Chang *et al.*, Shen *et al.*). To ensure comparability, all analyses were performed across the HR+ breast cancer cohort. Kaplan-Meier survival analysis revealed that patients classified as low index group by all five indices exhibited significantly better OS (Figure S4E). The ROC curve analysis showed that the LMF\_index had superior predictive accuracy, with area under the curve (AUC) values of 0.735, 0.777, and 0.801 for 2-, 5-, and 8-year survival, respectively (Figure 4J). While the ferroptosis\_index and lipid metabolism\_index also exhibited AUC values above 0.6 (Figure 4K-N), they were consistently lower than those of the LMF\_index. Moreover, the C-index of the LMF\_index was 0.748, outperforming all other ferroptosis\_indices and lipid metabolism\_indices (Figure 4O). Additionally, all genes in the LMF\_index panel—except UGT2B4—showed a positive correlation with ferroptosis scores, as well as with the activity of fatty acid oxidation and fatty acid synthesis pathways (Figure S5).

To further validate the prognostic utility of the LMF\_index across different clinical pathological subgroups, Kaplan-Meier survival analyses were performed. The results indicated that, except for N3, M1, and Stage IV subgroups, LMF\_index high patients had significantly shorter OS compared to LMF\_index low patients (Figure S6). Additionally, the distribution of LMF\_index across various clinical characteristics was examined. The findings demonstrated that patients aged over 70 had a significantly higher LMF\_index than those under 70. Similarly, patients with T4-stage tumors exhibited a higher LMF\_index than those with T1, T2, or T3-stage disease. Patients with distant metastasis (M1) and those with Stage IV disease had significantly higher LMF\_index values than their M0 and earlier-stage counterparts, respectively (Figure S7). In summary, the LMF\_index effectively stratifies HR+ breast cancer patients into prognostic subgroups, demonstrating superior predictive accuracy for OS compared to existing indices, with validation across multiple cohorts and clinical subgroups.

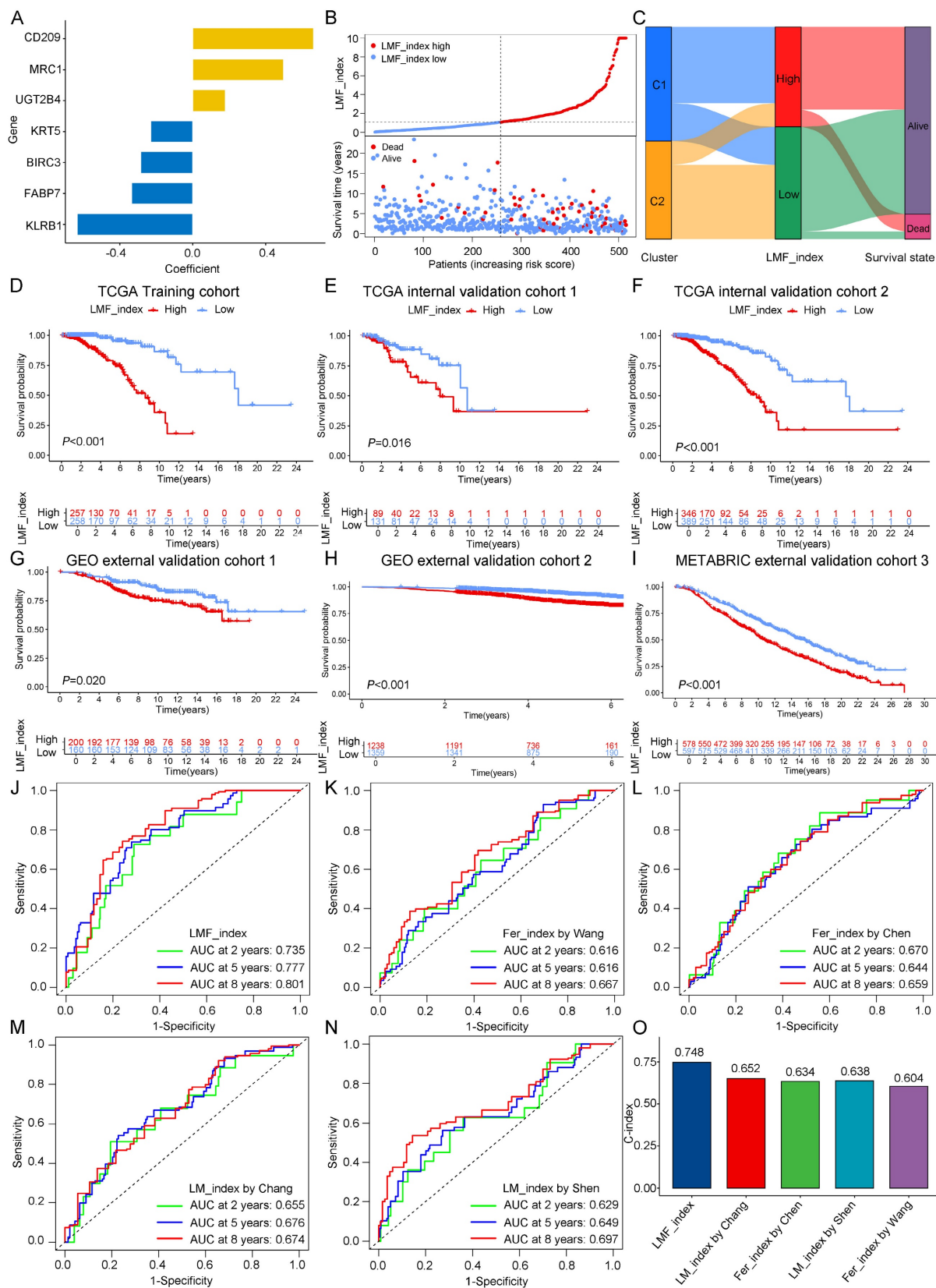


**Figure 4. Construction and validation of the LMF\_index and comparison with existing indices. (A)** LMF\_index panel genes and their corresponding regression coefficients identified by multivariate Cox regression analysis. **(B)** Distribution of LMF\_index and scatter plot of survival status. **(C)** Sankey diagram depicting the relationships among molecular clusters, LMF\_index, and survival status, providing a visual overview of patient classification and outcomes. **(D-I)** Kaplan-Meier survival curves for the TCGA training cohort, internal validation cohorts and external validation cohorts. **(J-N)** Time-dependent receiver operating characteristic (ROC) curve analysis comparing the area under the curve (AUC) values at 2, 5, and 8 years for the LMF\_index and existing indices. **(O)** Comparison of the concordance index (C-index) across different indices, demonstrating the overall predictive performance of each index in terms of concordance with actual outcomes.

### 3.4. Independent prognostic analysis of the LMF\_index and nomogram construction

To assess whether the LMF\_index serves as an independent prognostic factor for HR+ breast cancer, univariate and multivariate Cox regression analyses were performed, incorporating key clinical pathological variables including age, stage, T stage, N stage, and M stage. Univariate Cox regression analysis revealed that age (hazard ratio (HR) = 1.048, 95% confidence interval (CI) [1.029–1.067],  $P < 0.001$ ), stage (HR = 1.694, 95% CI [1.279–2.244],  $P < 0.001$ ), M stage (HR = 5.179, 95% CI [2.662–10.076],  $P < 0.001$ ), N stage (HR = 1.369, 95% CI [1.090–1.720],  $P = 0.007$ ), T stage (HR = 1.322, 95% CI [1.006–1.738],  $P = 0.045$ ), and LMF\_index (HR = 1.116, 95% CI [1.084–1.149],  $P < 0.001$ ) were significantly associated with patient prognosis (Figure 5A). Multivariate Cox regression analysis further confirmed that age (HR = 1.054, 95% CI [1.034–1.074],  $P < 0.001$ ) and LMF\_index (HR = 1.113, 95% CI [1.078–1.150],  $P < 0.001$ ) were independent prognostic factors for HR+ breast cancer (Figure 5B).

To enhance the accuracy of survival predictions, a nomogram was constructed by integrating age and the LMF\_index. Calibration curve analysis demonstrated strong predictive performance, with the nomogram achieving a C-index of 0.797 (95% CI [0.741–0.853]), indicating a high level of concordance between predicted and actual survival outcomes (Figure 5C–D). Additionally, multi-variable ROC curve analysis showed that the nomogram exhibited the highest AUC values for 2-year, 5-year, and 8-year survival predictions, with AUCs of 0.763, 0.787, and 0.821, respectively, demonstrating its superior predictive capability compared to individual prognostic factors (Figure 5E–G). In summary, the LMF\_index was identified as an independent prognostic factor for HR+ breast cancer. Its integration into a nomogram significantly improves survival prediction, providing a valuable tool for individualized prognostic assessment.

### 3.5. Validation of LMF\_index in the Shanghai cohort and tissue microarray analysis

To further evaluate the stability and prognostic accuracy of LMF\_index, an external validation was performed using the Shanghai cohort, which included 482 HR+ breast cancer patients who received endocrine therapy. Based on the optimal cut-off value, patients were stratified into high LMF\_index and low LMF\_index groups. Kaplan-Meier survival analysis demonstrated that patients in the high LMF\_index group exhibited significantly worse OS compared to those in the low LMF\_index group (Figure 6A).

Moreover, ROC curve analysis revealed that the AUC value for 8-year OS prediction exceeded 0.6, further confirming the predictive reliability of LMF\_index in HR+ breast cancer (Figure 6B). Additionally, univariate and multivariate Cox regression analyses established LMF\_index as an independent prognostic factor for HR+ breast cancer patients (Figure 6C–D), highlighting its clinical relevance in prognostic assessment.

To further validate the prognostic significance of LMF\_index, mIHC staining was performed on breast cancer tissue microarrays to assess the expression levels of KRT5, UGT2B4, BIRC3, MRC1, CD209, FABP7, and KLRB1. The tissue microarray used in this study comprised samples from 136 breast cancer patients. However, during multiple staining experiments, five tissue spots were found to have detachment issues. As a result, a total of 131 breast cancer patients were included in the subsequent analysis. The LMF\_index was calculated based on the proportion of positively stained cells for the seven protein markers. Representative mIHC images demonstrated distinct expression differences between high and low LMF\_index groups (Figure 7A–B). Kaplan-Meier survival analysis further demonstrated that patients with a low LMF\_index had a more favorable prognosis (Figure 7C). Furthermore, ROC curve analysis showed that LMF\_index achieved an AUC of 0.76 in 8-year OS prediction, underscoring its potential as a robust prognostic biomarker (Figure 7D). Notably, LMF\_index was significantly associated with patient age and survival status (Figure 7E), further supporting its clinical relevance as a prognostic indicator. In conclusion, this study validated the LMF\_index in an independent external Shanghai cohort at the transcriptomic level and in a breast cancer tissue microarray at the protein level, confirming its reliability as a prognostic biomarker for HR+ breast cancer.

### 3.6. Analysis of expression levels of LMF\_index panel genes

To further investigate the expression characteristics of LMF\_index panel genes in breast cancer, we first analyzed their expression levels in normal breast tissue and HR+ breast cancer tissues using the UALCAN database. The results demonstrated that KRT5, UGT2B4, MRC1, CD209, and KLRB1 were significantly downregulated in HR+ breast cancer compared to normal breast tissue, whereas BIRC3 and FABP7 showed no significant differences in expression between the two groups (Figure S8). To further elucidate the distribution of these genes in different cell types, we analyzed scRNA-seq data from the GSE148673 dataset. UMAP

clustering classified the cells into 28 subpopulations, which were subsequently annotated into 9 major cell types (Figure 8A-C). Single-cell expression analysis revealed that KRT5 and FABP7 were highly enriched in tumor cells, UGT2B4 was predominantly expressed in epithelial cells, BIRC3 and KLRB1 were enriched in CD8+ T cells, while MRC1 and CD209 were highly

expressed in monocytes/macrophages (Figure 8D-J and Figure S9). These findings delineate the distinct expression patterns of LMF\_index panel genes in tumor cells and immune cells, providing valuable insights into their potential functional roles in tumor progression and immune regulation.

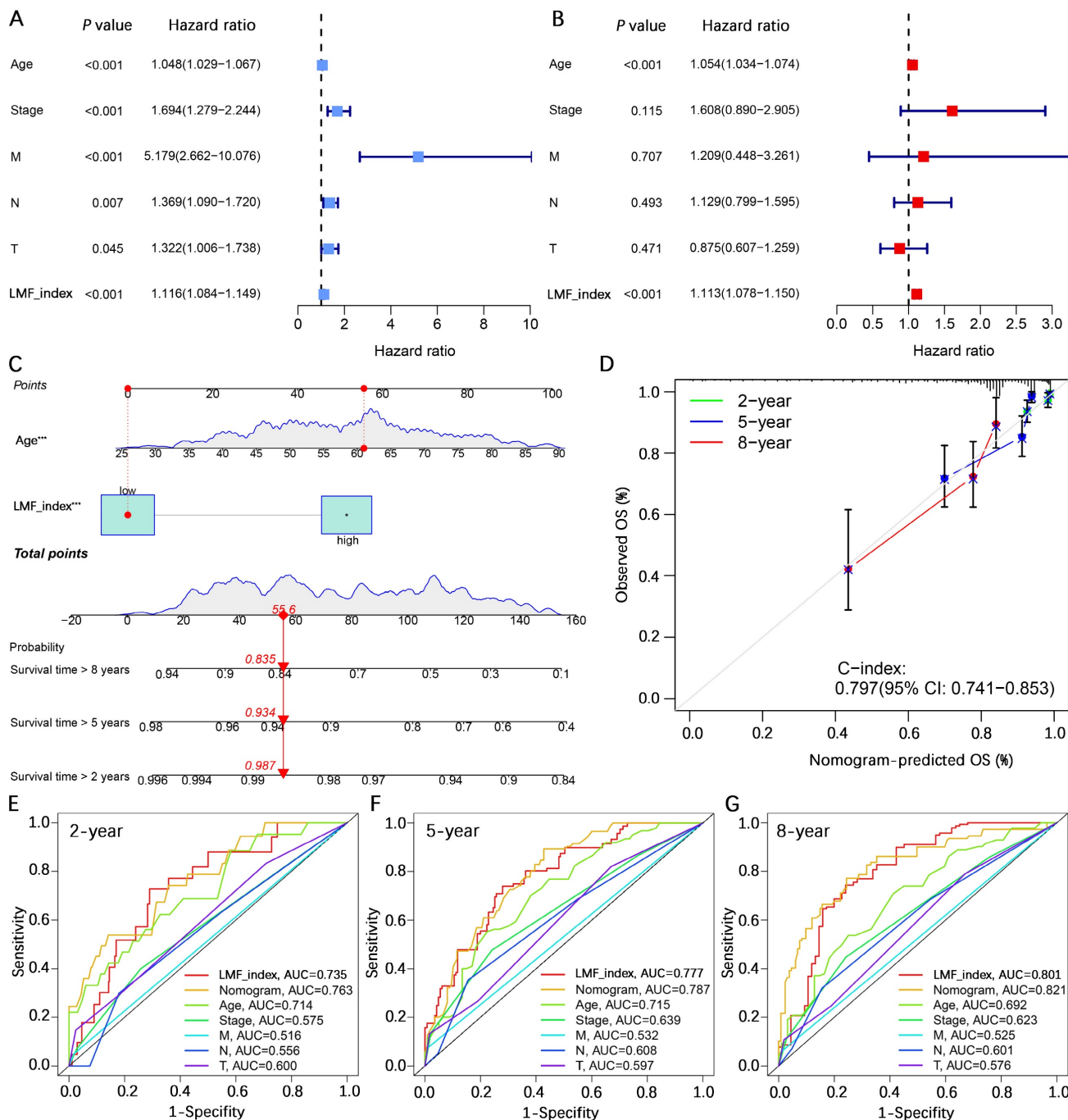


**Figure 5. Independent prognostic analysis of the LMF\_index and nomogram construction. (A-B)** Univariate and multivariate Cox regression analyses of clinical-pathological characteristics and LMF\_index. **(C)** Construction of a nomogram incorporating LMF\_index and clinical-pathological factors. **(D)** Calibration curves for assessing the accuracy of the nomogram in predicting outcomes. **(E-G)** Receiver operating characteristic (ROC) curve analysis of the nomogram, risk score, and clinical-pathological factors for predicting 2-year, 5-year, and 8-year survival.

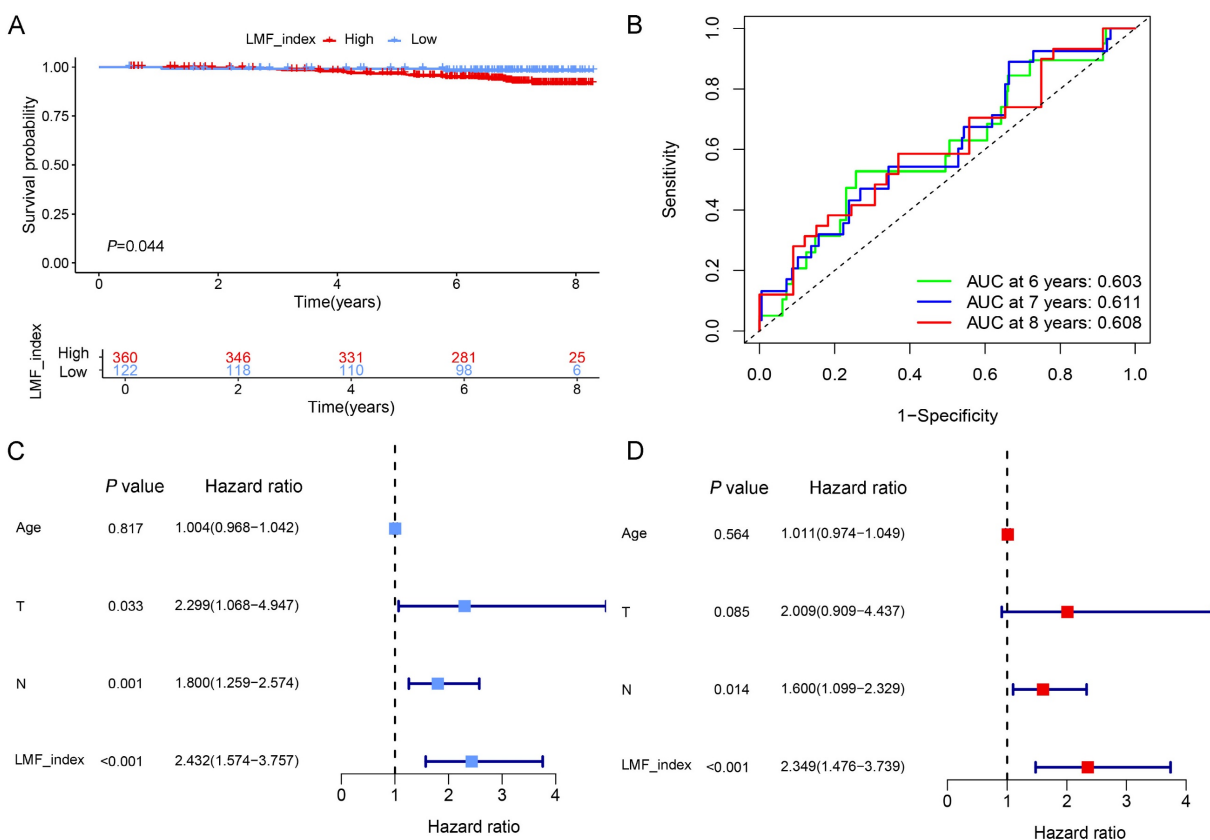


**Figure 6. Validation of the prognostic value of LMF\_index in the Shanghai cohort. (A)** Kaplan-Meier survival analysis comparing the LMF\_index low and high groups, using the optimal cut-off value. **(B)** Time-dependent receiver operating characteristic (ROC) curves of LMF\_index at 6, 7, and 8 years in the Shanghai cohort. **(C-D)** Univariate and multivariate Cox regression analyses of LMF\_index combined with clinical and pathological factors in the Shanghai cohort.

### 3.7. Immune landscape and immunotherapy sensitivity analysis

Recent studies have demonstrated that cell debris and lipid metabolites released during ferroptosis can enhance tumor-specific immune responses by activating antigen-presenting cells and promoting T cell activation[27]. To further explore the mechanistic basis by which the LMF\_index functions as an independent prognostic factor, we investigated the relationships among the LMF\_index, ferroptosis, and immune cell infiltration in HR+ breast cancer samples from the TCGA cohort. Correlation analysis revealed that the LMF\_index was negatively associated with both the ferroptosis score and immune infiltration score, whereas ferroptosis and immune infiltration scores were positively correlated with each other (Figure S10A-C). These findings suggest that the improved prognosis observed in patients with a low LMF\_index may be attributed, at least in part, to enhanced ferroptotic activity and more robust immune cell infiltration. ACSL4 has been recognized as a key determinant of ferroptosis sensitivity and has been associated with increased CD8+ T cell infiltration and improved response to

ICIs[49]. In contrast, GPX4 is known to suppress ferroptosis by detoxifying lipid peroxides[50]. To further explore their spatial distribution, we employed PanCK staining to distinguish epithelial and stromal regions in tissue microarrays and performed mIHC for PanCK, CD8, ACSL4 and GPX4 (Figure S10D-E). The results showed no significant difference in the distribution of ACSL4+ cells between epithelial and stromal regions, whereas GPX4+ cells were significantly more abundant in epithelial compartments (Figure S10F). Notably, ACSL4+ cell density was significantly higher in the low LMF\_index group compared to the high LMF\_index group, while GPX4+ cell distribution did not differ significantly between the two groups (Figure S10G). Further correlation analysis revealed a positive association between ACSL4+ cells and CD8+ T cell infiltration, while no such correlation was observed for GPX4+ cells (Figure S10H-I). These data suggest that patients in the low LMF\_index group exhibit higher ACSL4 expression, indicating increased ferroptosis sensitivity, which may contribute to greater CD8+ T cell infiltration and enhanced anti-tumor immunity.

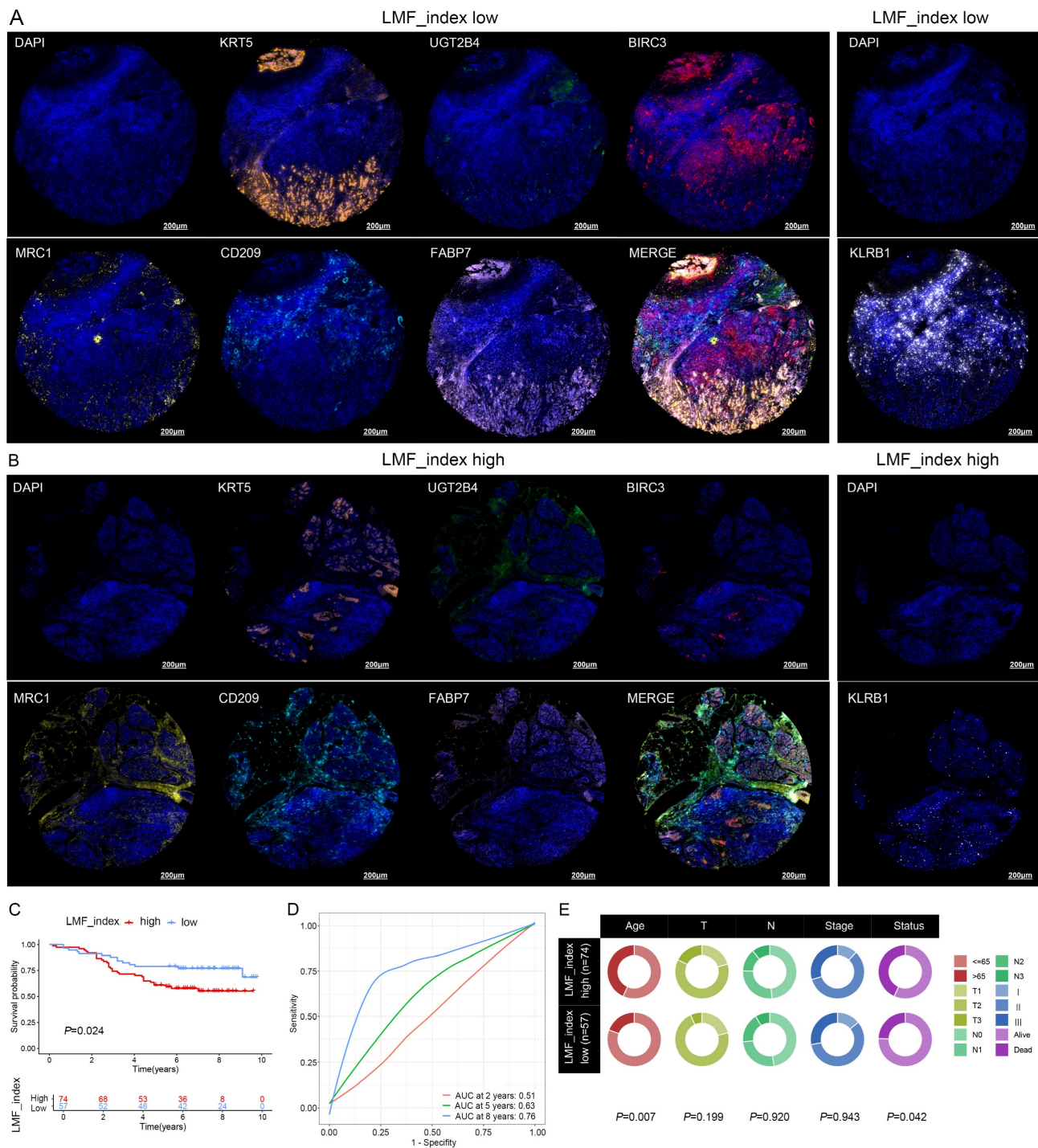
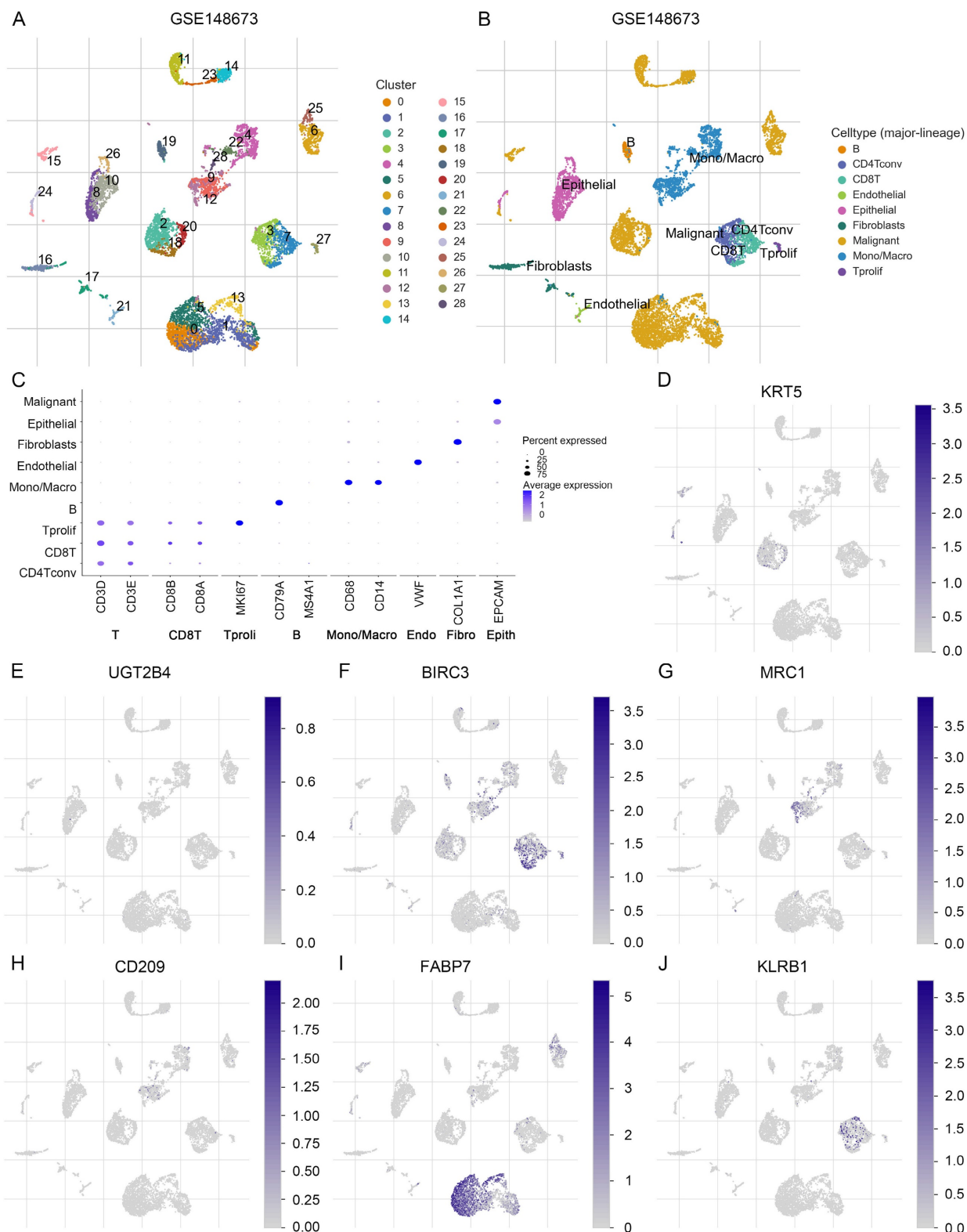


**Figure 7. Prognostic value of LMF\_index in breast cancer tissue microarray. (A)** Representative images of KRT5, UGT2B4, BIRC3, MRC1, CD209, FABP7, and KLRB1 based on multiplex immunohistochemistry (mIHC) staining in the LMF\_index low group. **(B)** Representative images of KRT5, UGT2B4, BIRC3, MRC1, CD209, FABP7, and KLRB1 based on mIHC staining in the LMF\_index high group. **(C)** Kaplan-Meier overall survival (OS) analysis comparing the LMF\_index low and high groups, using the optimal cut-off value. **(D)** Time-dependent receiver operating characteristic (ROC) curves of the LMF\_index for 2-, 5-, and 8-year OS. **(E)** Circo plot illustrating the distribution of different clinical factors between the LMF\_index low and high groups.



Next, multiple algorithmic analyses revealed a positive correlation between the LMF\_index and

macrophage infiltration, whereas it was negatively correlated with the infiltration of CD8+ T cells, B cells,

and natural killer (NK) cells (**Figure S11A**). Given the association between the LMF\_index and immune cell infiltration, we further explored differences in the immune microenvironment between LMF\_index high and LMF\_index low groups in HR+ breast cancer patients. ESTIMATE analysis revealed that LMF\_index low patients exhibited higher stromal scores, immune scores, and total ESTIMATE scores compared to LMF\_index high patients, suggesting a more active immune cell infiltration and lower tumor purity in the LMF\_index low group (**Figure S11B**). Specifically, LMF\_index low patients displayed increased infiltration of naïve B cells, memory B cells, plasma cells, CD8+ T cells, resting memory CD4+ T cells, follicular helper T cells, monocytes, M1 macrophages, resting dendritic cells (DCs), and neutrophils, compared to their LMF\_index high counterparts. Conversely, LMF\_index high patients exhibited higher infiltration of resting NK cells, M0 macrophages, and M2 macrophages, indicative of a more immunosuppressive TME (**Figure S11C**). Furthermore, ssGSEA analysis confirmed that LMF\_index low patients not only demonstrated higher immune cell infiltration but also exhibited enhanced immune-related functional activities, including chemokine receptor signaling, immune checkpoint signaling, human leukocyte antigen (HLA) signaling, and type II interferon response (**Figure S11D**). Additionally, mIHC analysis of the breast cancer tissue microarray confirmed that CD8+ T cell, CD68+ (M0-like) macrophages, and CD68+CD163- (M1-like) macrophages infiltration levels were significantly higher in the LMF\_index low group compared to the LMF\_index high group. In contrast, no statistically significant difference was observed in CD68+CD163+ (M2-like) macrophages infiltration between the two groups (**Figure 9A-E**).

The efficacy of antitumor therapies in breast cancer is significantly influenced by the TME, which plays a crucial role in determining patient prognosis and treatment response, particularly in immunotherapy[51, 52]. Given that the LMF\_index reflects the level of immune cell infiltration within the TME, we further investigated its role in predicting immunotherapy response in HR+ breast cancer. We first analyzed its correlation with immune checkpoint expression in HR+ breast cancer. As shown in **Figure S11E**, the LMF\_index was correlated with the expression levels of various immune checkpoints in HR+ breast cancer. Subgroup analysis revealed that LMF\_index low patients exhibited significantly higher expression of PD-1, PD-L1, and CTLA4 compared to LMF\_index high patients (**Figure S11F-H**), suggesting that LMF\_index low tumors may be more sensitive to ICIs. Additionally, mIHC

analysis of the tissue microarray confirmed that PD-L1 expression levels were significantly higher in the LMF\_index low group compared to the LMF\_index high group (**Figure 9A, F**). Further validation was performed using the IPS, a biomarker-based scoring system that predicts tumor responsiveness to ICIs, with higher IPS scores indicating a better immunotherapy response[53]. Our findings demonstrated that LMF\_index low patients had significantly higher IPS than LMF\_index high patients (**Figure 9G-J**), reinforcing the notion that LMF\_index low tumors are more likely to benefit from ICIs therapy. Additionally, data from the I-SPY2 clinical trial were analyzed to evaluate real-world neoadjuvant immunotherapy response. HR+ breast cancer patients with LMF\_index low exhibited a significantly higher pCR rate following neoadjuvant immunotherapy than LMF\_index high patients ( $P < 0.05$ , **Figure 9K**), further highlighting the potential clinical utility of the LMF\_index in guiding immunotherapy selection. In summary, the LMF\_index is closely associated with the tumor immune microenvironment, with LMF\_index low patients exhibiting higher immune infiltration, increased immune checkpoint expression, and greater responsiveness to immune checkpoint inhibitors, as confirmed by IPS analysis and neoadjuvant immunotherapy outcomes in the I-SPY2 trial.

### **3.8. KLRB1 expression correlates with immune cell infiltration and may serve as a biomarker for immunotherapy response**

Single-cell expression analysis of LMF\_index panel genes revealed that BIRC3 and KLRB1 were predominantly enriched in T cells. Differential expression analysis between normal breast tissue and HR+ breast cancer tissue showed significantly lower KLRB1 expression in tumor tissues, whereas BIRC3 expression exhibited no significant difference. Furthermore, univariate Cox regression analysis identified KLRB1 as a protective factor ( $HR < 1$ ,  $P < 0.05$ ), with its expression negatively correlated with LMF\_index ( $R = -0.432$ ,  $P < 0.001$ ) (**Figure S12A**). Paired breast cancer tissue analysis confirmed that KLRB1 expression was significantly lower in tumors compared to adjacent normal tissues (**Figure S12B**). The mIHC results showed that patients with high KLRB1 expression had better prognosis and higher PD-L1 expression levels (**Table 1**). Survival analysis using the Kaplan-Meier Plotter database further demonstrated that higher KLRB1 expression was associated with significantly better OS and RFS in HR+ breast cancer patients (**Figure S12C**).

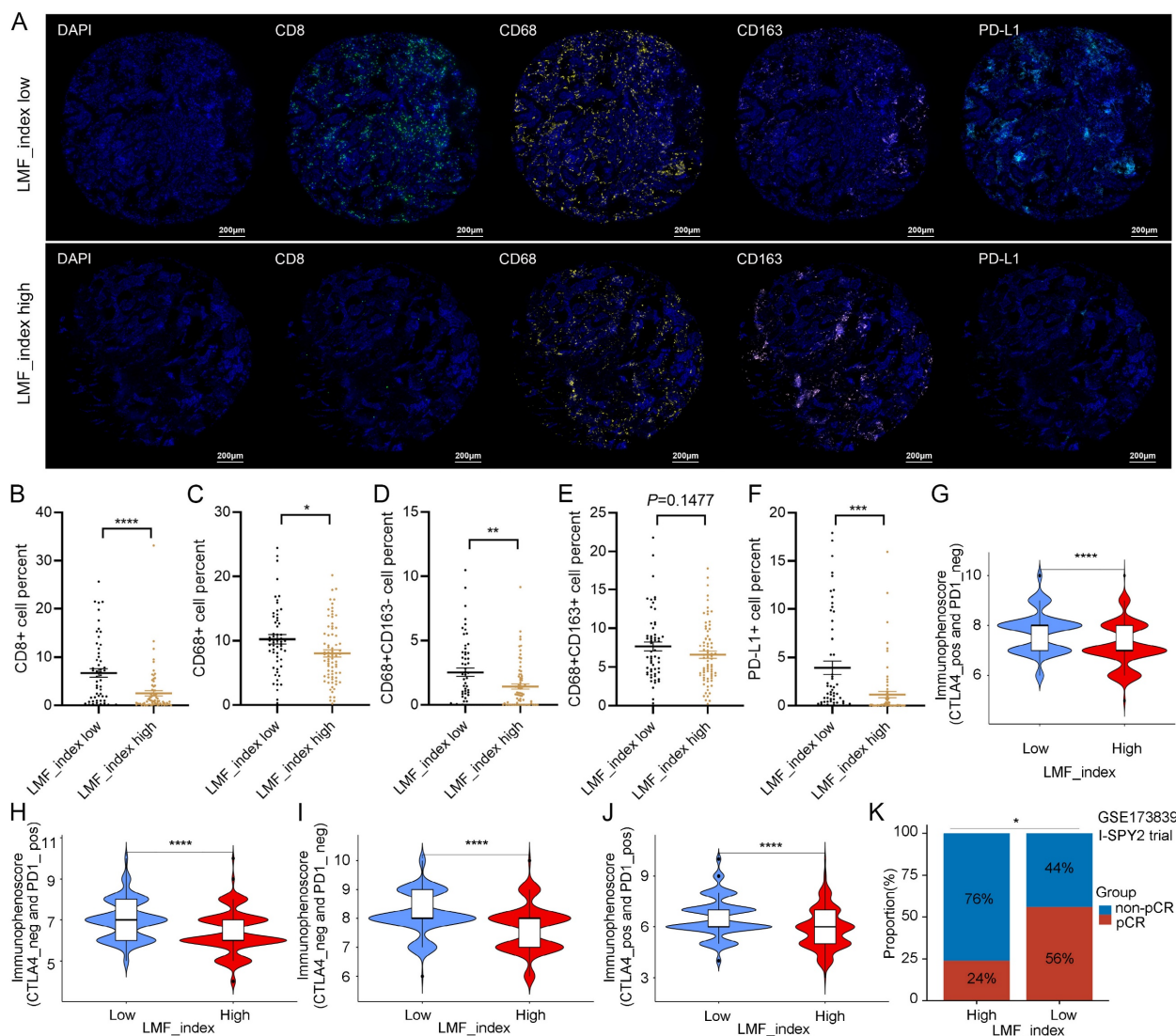


**Figure 9. Immune cell infiltration and immunotherapy sensitivity analysis in different LMF\_index groups. (A)** Representative multiplex immunohistochemistry (mIHC) images showing CD8, CD68, CD163, and PD-L1 expression in LMF\_index low and high groups. **(B-F)** Quantification of immune cell infiltration, comparing CD8+ T cells, CD68+ (M0-like) macrophages, CD68+CD163- (M1-like) macrophages, CD68+CD163+ (M2-like) macrophages, and PD-L1+ cells between LMF\_index low and high groups. **(G-J)** Comparison of immunophenoscore (IPS) between LMF\_index low and high groups. **(K)** Comparison of pathological complete response (pCR) rates between LMF\_index low and high patients who received neoadjuvant immunotherapy in the GSE173839 dataset. \* $P < 0.05$ ; \*\* $P < 0.01$ ; \*\*\* $P < 0.001$ ; \*\*\*\* $P < 0.0001$ .

To investigate the role of KLRB1 in the tumor immune microenvironment, we examined its correlation with immune cell infiltration. Heatmap analysis indicated that KLRB1 expression was positively correlated with multiple immune cell populations, including T cells, B cells, and macrophages (Figure S12D). H&E staining further validated that breast cancer tissues with high KLRB1 expression exhibited increased lymphocyte infiltration (Figure S12E). To further assess the relationship between KLRB1 expression and immune cell infiltration, mIHC staining was performed on breast cancer tissue microarrays, targeting PanCK, KLRB1, CD8, CD68, CD163, and PD-L1. Representative images in Figure 10A and Figure S12F demonstrated distinct immune infiltration patterns

between patients with low and high KLRB1 expression. Protein expression levels were quantified based on the proportion of marker-positive cells, and survival analysis was conducted accordingly. The results indicated that patients with a higher proportion of KLRB1-positive cells exhibited significantly better prognosis (Figure 10B). Similarly, higher proportions of CD8+ T cells (Figure 10C) and CD68+CD163- macrophages (Figure 10E) were associated with improved survival outcomes. In contrast, CD68+ cells and CD68+CD163+ macrophages showed no significant correlation with prognosis (Figures 10D, F). Correlation analysis further revealed that KLRB1+ cells were positively associated with CD8+ T cells, CD68+ macrophages, CD68+CD163- macrophages, and PD-L1+ cells

(Figure 10G). Subgroup analysis demonstrated that patients with high KLRB1 expression exhibited significantly higher infiltration levels of CD8+ T cells, M0 macrophages, and M1 macrophages compared to those with low KLRB1 expression (Figure 10H-J). However, M2 macrophage infiltration levels did not differ significantly between the two groups (Figure 10K). Furthermore, spatial analysis based on PanCK expression revealed that KLRB1 expression was significantly higher in the stromal compartment than in the epithelial compartment, suggesting its predominant presence in immune cells (Figure 10L). Notably, Kaplan-Meier survival analysis of immunotherapy-treated patients from the Kaplan-Meier Plotter database demonstrated that high KLRB1 expression was associated with prolonged OS in patients receiving PD-1, PD-L1, or CTLA-4 blockade therapy (Figure 10M-O). These findings highlight KLRB1 as a key regulator of the immune microenvironment, demonstrating its strong correlation with CD8+ T cell and M1 macrophage infiltration. Moreover, KLRB1 may serve as a potential prognostic biomarker and predictor of immunotherapy response, offering novel insights for optimizing immunotherapeutic strategies.

#### 4. Discussion

In the present study, we identified distinct LMF-related molecular clusters in HR+ breast cancer, providing new insights into the prognostic and immunological diversity. Our findings reveal that patients in cluster 1, characterized by higher TMB, more active proliferative signaling (PI3K/AKT/mTOR), and elevated Ki-67 expression, exhibited more aggressive tumor features and relatively poorer clinical outcomes. In contrast, cluster

2 demonstrated greater immune cell infiltration, higher expression of immune checkpoints (PD-1, PD-L1, and CTLA-4), and a more favorable prognosis. These results are consistent with previous studies suggesting that high TMB and elevated proliferation markers are associated with more aggressive tumor behavior in HR+ breast cancer[54, 55], whereas robust tumor-infiltrating lymphocytes (TILs) and higher immune checkpoint expression often correlate with improved outcomes and responsiveness to immunotherapy in various solid tumors[56].

Building upon the molecular clustering analysis, we developed the LMF\_index and conducted comprehensive validation across two internal and four external validation cohorts. Further analysis demonstrated that the LMF\_index effectively stratifies HR+ breast cancer patients into LMF\_index low and LMF\_index high subgroups. Notably, patients in the LMF\_index low group exhibited significantly better OS than those in the LMF\_index high group. This trend was consistently observed across various clinicopathological subgroups, further reinforcing the robustness of the LMF\_index as a prognostic classifier. Moreover, multivariate Cox regression analysis confirmed that the LMF\_index is an independent prognostic factor for HR+ breast cancer, highlighting its potential clinical utility. Compared to previously established lipid metabolism-related and ferroptosis-related indices[28-31], the LMF\_index integrates two tightly linked biological processes, demonstrating superior predictive accuracy and stability in prognosis assessment. ROC curve analysis showed that the AUC values for 2-, 5-, and 8-year survival predictions were consistently higher for the LMF\_index than for other indices[28-31], indicating its enhanced long-term prognostic capability.

**Table I.** Association between KLRB1 expression and clinicopathological characteristics in breast cancer tissue microarray.

Characteristics	KLRB1 low (n=66)	KLRB1 high (n=65)	P value	Statistic	Method
Age, median (IQR)	60 (50.25, 71)	54 (49, 67)	0.111	-	Wilcoxon
T, n (%)			0.565	1.1425	Chisq test
T1	15 (11.5%)	12 (9.2%)			
T2	41 (31.3%)	46 (35.1%)			
T3	10 (7.6%)	7 (5.3%)			
N, n (%)			0.186	4.8124	Chisq test
N0	33 (25.2%)	30 (22.9%)			
N1	21 (16%)	14 (10.7%)			
N2	6 (4.6%)	14 (10.7%)			
N3	6 (4.6%)	7 (5.3%)			
Stage, n (%)			0.276	2.5777	Chisq test
I	9 (6.9%)	8(6.1%)			
II	42 (32.1%)	34 (26%)			
III	15 (11.5%)	23 (17.6%)			
Status, n (%)			0.033	4.5466	Chisq test
Dead	29 (22.1%)	17 (13%)			
Alive	37 (28.2%)	48 (36.6%)			
PD-L1+ cells percent, median (IQR)	0.075 (0.02, 0.652)	1.25 (0.15, 5.68)	< 0.001	-	Wilcoxon

A

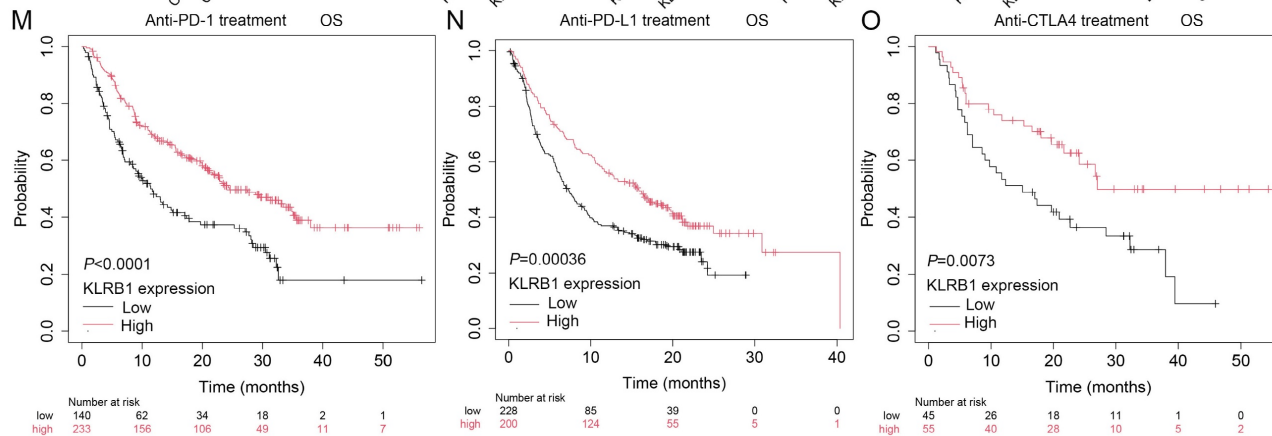
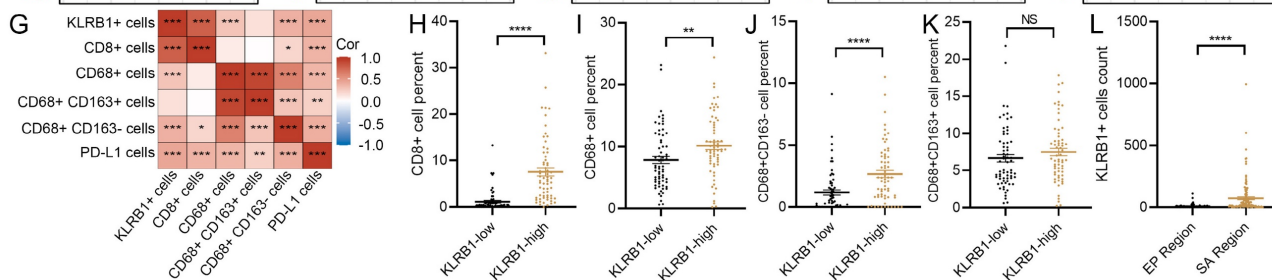
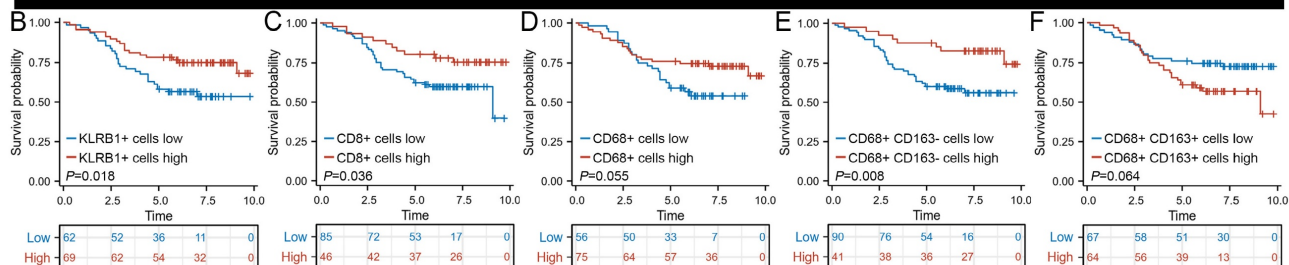
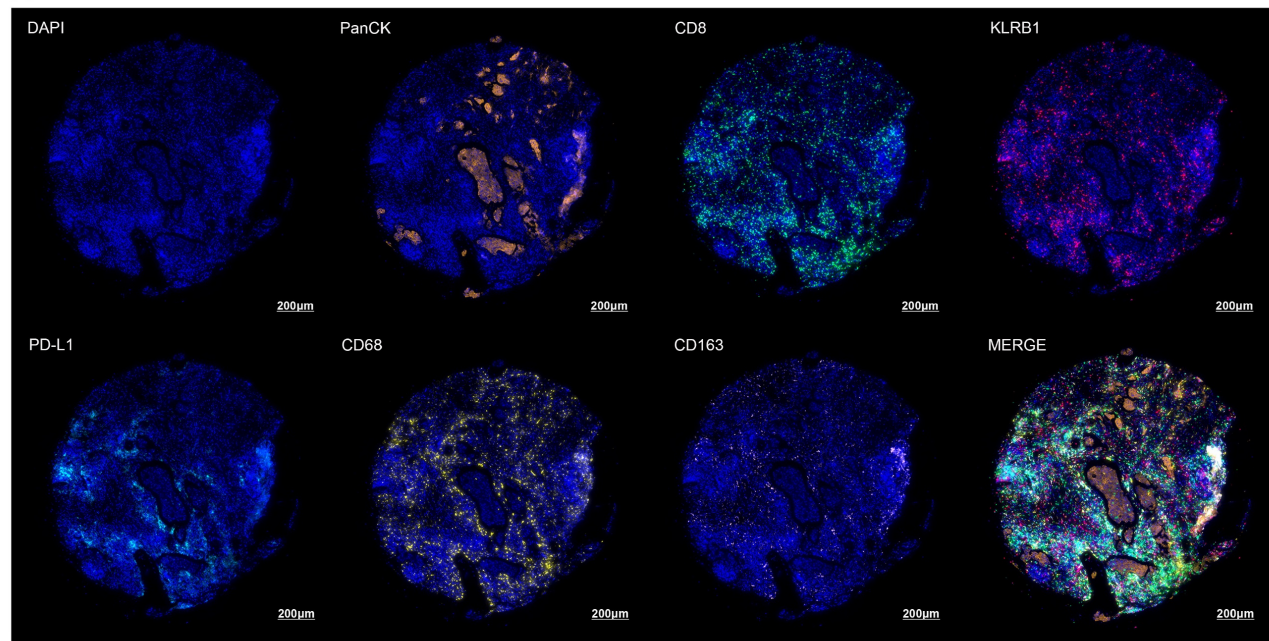


**Figure 10. KLRB1 expression and immune cell infiltration analysis in breast cancer tissue microarray. (A)** Representative multiplex immunohistochemistry (mIHC) images showing PanCK, CD8, KLRB1, PD-L1, CD68, and CD163 expression in the KLRB1 high group. **(B-F)** Kaplan-Meier overall survival (OS) analysis comparing the infiltration levels of KLRB1+ cells, CD8+ T cells, CD68+ (M0-like) macrophages, CD68+CD163- (M1-like) macrophages, and CD68+CD163+ (M2-like) macrophages. **(G)** Correlation heatmap analysis of the percentages of KLRB1+ cells, CD8+ T cells, CD68+ (M0-like) macrophages, CD68+CD163- (M1-like) macrophages, and CD68+CD163+ (M2-like) macrophages, and PD-L1+ cells. **(H-K)** Infiltration level differences in CD8+ T cells, CD68+ (M0-like) macrophages, CD68+CD163- (M1-like) macrophages, and CD68+CD163+ (M2-like) macrophages between KLRB1+ cells high and low breast cancer patients. **(L)** Differential analysis of KLRB1+ cells between stromal and epithelial regions. **(M-O)** Kaplan-Meier overall survival analysis based on KLRB1 expression levels in patients receiving PD-1 inhibitors, PD-L1 inhibitors, and CTLA4 inhibitors.

Furthermore, C-index analysis confirmed that the LMF\_index outperforms existing lipid metabolism and ferroptosis-related indices in predicting HR+ breast cancer prognosis[28-31], highlighting its potential for clinical application. Notably, in contrast to previous lipid metabolism or ferroptosis indices, our LMF\_index was further validated in our independent Shanghai cohort and breast cancer tissue microarray, providing additional evidence of its reliability and clinical applicability. These results further support the LMF\_index as a robust prognostic biomarker with the potential for real-world clinical implementation in HR+ breast cancer.

The LMF\_index panel consists of seven key genes: KRT5, UGT2B4, BIRC3, MRC1, CD209, FABP7, and KLRB1. These genes were identified through a rigorous selection process, including LASSO regression and multivariate Cox analysis, to ensure their prognostic significance and functional relevance in HR+ breast cancer. Keratin 5 (KRT5) is a member of the keratin family, highly expressed in basal-like breast cancer and commonly used as a marker for basal-like subtype identification[57]. KRT5+ cells exhibit strong cancer stem cell (CSC) properties, which have been associated with endocrine therapy resistance and poor prognosis in ER+ breast cancer[58, 59]. Additionally, studies suggest that KRT5- $\beta$ -catenin interaction plays a critical role in maintaining the malignant phenotype of breast cancer cells, and targeting this pathway may serve as a novel therapeutic strategy[58]. UGT2B4, a member of the UDP-glucuronosyltransferase (UGT) family, plays a pivotal role in hepatic metabolism and drug biotransformation by catalyzing the glucuronidation of various endogenous and exogenous substrates[60]. Emerging evidence indicates that UGT2B4 contributes to doxorubicin resistance in breast cancer cells, potentially through somatic mutations that impair its normal enzymatic function or alter its expression[61, 62]. However, the underlying molecular mechanisms driving this resistance remain incompletely understood. Beyond its role in drug metabolism, UGT2B4 has been identified as a downstream target of peroxisome proliferator-activated receptor alpha (PPAR $\alpha$ ), implicating it in lipid and cholesterol metabolism[63]. As such, UGT2B4 is increasingly recognized as a key regulator of metabolic homeostasis, often referred to as a “lipid controller”[64]. Recent transcriptomic analyses have further expanded the biological significance of UGT2B4 in cancer. A study by Wang *et al.* identified UGT2B4 as a characteristic gene of ferroptosis-related molecular subtypes[65]. This observation is consistent with our current findings and supports the notion that UGT2B4 may serve a dual function—participating in

both lipid metabolic reprogramming and the regulation of ferroptosis—thereby contributing to tumor progression and therapeutic response. BIRC3, a member of the inhibitor of apoptosis protein (IAP) family, primarily regulates cell survival by modulating the NF- $\kappa$ B signaling pathway to inhibit apoptosis[66]. In breast cancer, BIRC3 upregulation has been associated with enhanced tumor cell survival and doxorubicin resistance[67]. Notably, a study by Feng *et al.* identified BIRC3 as a protective factor in breast cancer patients[68], which is consistent with the findings of this study. MRC1 is primarily expressed in M2 macrophages and plays a crucial role in shaping an immunosuppressive TME. In colorectal cancer liver metastases, highly metabolically active MRC1+CCL18+ M2 macrophages have been identified and are associated with poor response to neoadjuvant chemotherapy[69]. In breast cancer, TAp73 expression is negatively correlated with the accumulation of pro-tumorigenic MRC1+ macrophages in patient samples. Mechanistically, TAp73 regulates the accumulation and phenotype of MRC1+ macrophages by suppressing the NF- $\kappa$ B signaling pathway[70]. High MRC1 expression may indicate the enrichment of M2 macrophages within the TME, suggesting an enhanced immunosuppressive state, which could influence patient response to immunotherapy. CD209 is primarily expressed in DCs and plays a key role in antigen presentation and immune regulation[71]. In breast cancer, CD209 may influence the efficacy of ICIs by modulating DCs function. Fatty acid-binding proteins (FABPs) constitute a family of intracellular lipid chaperones that facilitate the trafficking and utilization of long-chain fatty acids within cells. Among them, FABP7 has garnered attention for its multifaceted role in lipid metabolism and cancer biology[72, 73]. FABP7 binds oleic acid (OA) to form FABP7-OA complex, which promotes the formation of nuclear lipid droplets, thereby contributing to lipid storage and signaling regulation[74]. Beyond fatty acid transport, FABP7 has also been recognized as a novel sterol transfer protein that mediates cholesterol efflux from lysosomes to the cytoplasm, playing a key role in maintaining intracellular cholesterol homeostasis[75]. In the context of cancer, FABP7 has been implicated in metabolic reprogramming of breast cancer cells, where it promotes glycolysis and lipid droplet accumulation, supporting tumor growth and survival[76]. Interestingly, FABP7 expression is frequently downregulated in breast cancer tissues, and it has been proposed as a potential biomarker for predicting response to neoadjuvant chemotherapy [77]. Moreover, recent evidence suggests a more nuanced role for FABP7 in the tumor immune

microenvironment. Specifically, FABP7 upregulation in immunotherapy-resistant tumors has been shown to confer protection against ferroptosis by modulating lipid composition and mitochondrial function[78]. KLRB1 encodes CD161, which is predominantly expressed on NK cells and CD8+ T cells, playing a crucial role in antitumor immunity[79]. In this study, we found that high KLRB1 expression was associated with increased infiltration of CD8+ T cells and M1 macrophages, and patients with elevated KLRB1 levels exhibited a better response to immunotherapy. These findings suggest that KLRB1 may serve as a potential predictive biomarker for immunotherapy efficacy in HR+ breast cancer. The LMF\_index panel genes encompass key biological processes, including tumor stemness, metabolic regulation, apoptosis and survival, and immune modulation within the TME. Their collective function may influence HR+ breast cancer progression and response to immunotherapy.

The LMF\_index developed in this study effectively stratifies HR+ breast cancer patients and is closely associated with TME characteristics. HR+ breast cancer is typically characterized by an immune-cold TME, with low immune cell infiltration and reduced immune activation[16]. However, emerging studies suggest that the TME of HR+ breast cancer exhibits plasticity, and not all patients present with the same immune profile. For instance, a subset of HR+ breast cancer patients demonstrates higher infiltration of CD8+ T cells and M1 macrophages, contributing to a more robust anti-tumor immune response[80, 81]. In this study, ESTIMATE analysis revealed that patients in the LMF\_index low group exhibited significantly higher immune and stromal scores than those in the LMF\_index high group, indicating a TME enriched with immune-active components in the former, while the latter exhibited higher tumor purity. Furthermore, LMF\_index low patients displayed increased levels of CD8+ T cells, M1 macrophages, plasma cells, and follicular helper T cells, whereas LMF\_index high patients were enriched in M2 macrophages and resting NK cells. These findings align with the classical TME paradigm, where M1 macrophages and CD8+ T cells are associated with an enhanced anti-tumor immune response, whereas M2 macrophages contribute to tumor progression and immune suppression[82].

ICIs have demonstrated significant efficacy in TNBC; however, their clinical progress in HR+ breast cancer has been relatively slow[16]. The KEYNOTE-756 and CheckMate 7FL trials have shown that ICIs combined with neoadjuvant chemotherapy can improve the pCR rate in HR+ breast cancer patients[18, 19]. Nevertheless, identifying HR+ breast cancer patients who are most likely to benefit from

immunotherapy remains a critical clinical challenge. In this study, we assessed the ability of the LMF\_index to predict ICIs response using the IPS. The results showed that patients with a low LMF\_index exhibited significantly higher IPS scores than those with a high LMF\_index, suggesting that the LMF\_index low group may be more responsive to PD-1/PD-L1 inhibitors. Furthermore, analysis of the I-SPY2 clinical trial dataset revealed that patients in the LMF\_index low group had a significantly higher pCR rate following neoadjuvant immunotherapy compared to those in the LMF\_index high group, further validating the predictive value of the LMF\_index for immunotherapy outcomes. Additionally, mIHC analysis demonstrated that KLRB1 expression was higher in HR+ breast cancer patients with a low LMF\_index, and patients with high KLRB1 expression also exhibited elevated PD-L1 levels. These findings align with previous studies indicating that patients with high PD-L1 expression have a better response to immunotherapy[18, 19]. Therefore, the LMF\_index holds potential as a biomarker for immunotherapy selection in HR+ breast cancer, aiding in patient stratification and enhancing the precision of immunotherapy strategies.

This study has several strengths. First, we identified two distinct molecular subtypes of HR+ breast cancer, providing new insights into tumor heterogeneity and immune microenvironment characteristics. Second, we developed the LMF\_index, a robust prognostic biomarker, which was validated across multiple independent cohorts, including our Shanghai cohort, demonstrating superior prognostic performance compared to existing indices. Additionally, protein-level validation using mIHC on tissue microarrays further strengthens the reliability and applicability of this biomarker. Third, our findings indicate that patients with a low LMF\_index exhibit a more active immune microenvironment and may derive greater benefit from ICIs, underscoring its potential role in guiding immunotherapy strategies. Furthermore, we identified KLRB1 as a key immune-related gene, positively correlated with CD8+ T cell and M1 macrophage infiltration, and associated with improved immunotherapy response, making it a promising biomarker for patient stratification in clinical practice.

Despite these strengths, several limitations should be acknowledged. First, although the LMF\_index was validated across multiple cohorts and at the protein level using tissue microarrays, its clinical utility requires further confirmation through prospective clinical trials and larger datasets. Second, while this study demonstrates that the LMF\_index can predict immunotherapy efficacy, additional

prospective clinical studies are needed to validate its role in guiding treatment decisions. Third, although we identified strong associations between the LMF\_index, immune landscape features, and patient prognosis, further functional validation is warranted. Specifically, *in vitro* and *in vivo* experiments are needed to elucidate the mechanistic roles of key LMF\_index genes—such as BIRC3, FABP7, and UGT2B4—in regulating lipid metabolism, ferroptosis sensitivity, and immune evasion. Fourth, although bulk transcriptomic analysis provides valuable insights, future studies integrating single-cell metabolomics with single-cell transcriptomic data are warranted to further validate and refine the biological relevance of the LMF\_index in HR+ breast cancer at a higher cellular resolution. Finally, this study primarily focused on HR+ breast cancer; future research should investigate whether this integrative index can be applied to other breast cancer subtypes or malignancies to expand its clinical relevance.

## 5. Conclusion

In conclusion, this study identified distinct LMF-related molecular clusters in HR+ breast cancer, each exhibiting unique prognostic and immune characteristics. Furthermore, the LMF\_index represents a promising prognostic and predictive biomarker for HR+ breast cancer, offering potential guidance for immunotherapy stratification. However, further validation through functional studies and prospective clinical trials is essential to establish its broader clinical applicability.

## Abbreviations

AIs: aromatase inhibitors; AUC: area under the curve; CSC: cancer stem cell; C-index: concordance index; CI: confidence interval; CDF: cumulative distribution function; CDK4/6: cyclin-dependent kinase 4/6; DCs: dendritic cells; DEGs: differential expression genes; DFS: disease-free survival; mDNAsi: DNA stemness index; ER: estrogen receptor; ER $\alpha$ : estrogen receptor alpha; GO: gene ontology; IC50: half-maximal inhibitory concentration; HR: hazard ratio; H&E: hematoxylin and eosin; HR+: hormone receptor-positive; HER2: human epidermal growth factor receptor 2; HLA: human leukocyte antigen; ICIs: immune checkpoint inhibitors; IPS: immunophenoscores; KEGG: kyoto encyclopedia of genes and genomes; LASSO: least absolute shrinkage and selection operator; LMF: lipid metabolism and ferroptosis; NK: natural killer; PFS: progression-free survival; OA: oleic acid; OS: overall survival; pCR: pathological complete response; PCA: principal component analysis; PR: progesterone receptor; ROC: receiver operating characteristic; RFS:

recurrence-free survival; RCB: residual cancer burden; mRNAsi: RNA stemness index; scRNA-seq: single-cell RNA sequencing; SERMs: selective estrogen receptor modulators; SERDs: selective estrogen receptor degraders; ssGSEA: single-sample gene set enrichment analysis; t-SNE: t-distributed stochastic neighbor embedding; TCGA-BRCA: the cancer genome atlas-breast invasive carcinoma; TCIA: the cancer immunome atlas; TNBC: triple-negative breast cancer; TISCH2: Tumor Immune Single-cell Hub 2; TME: tumor microenvironment; TMB: tumor mutational burden; UALCAN: University of Alabama at Birmingham Cancer data analysis portal.

## Supplementary Material

Supplementary figures.

<https://www.ijbs.com/v21p3968s1.pdf>

Supplementary tables.

<https://www.ijbs.com/v21p3968s2.xlsx>

## Acknowledgments

The authors sincerely acknowledge the publicly available databases that provided the data for this study. Additionally, we thank BioRender (<https://app.biorender.com>) for assisting in the creation of Figure 1.

## Funding

This study was supported by the Noncommunicable Chronic Diseases-National Science and Technology Major Project (2023ZD0502200), the National Natural Science Foundation of China (92459304, 82230058, 82472633), the Natural Science Foundation of Beijing City (7242115), the Joint innovative Fund of Beijing Natural Science Foundation and Changping District (L234004), the Special Research Fund for Central Universities, Peking Union Medical College (APL23100510010301045), CAMS Innovation Fund for Medical Sciences (CIFMS) (2021-12M-1-014), CAMS Innovation Fund for Medical Sciences (2022-12M-2-001), and CAMS Innovation Fund for Medical Sciences (2023-12M-2-004).

## Author contributions

All authors contributed to the study conception and design. Protocol/project development was assumed by Fei Ma, Haili Qian, and Yizhou Jiang. Material preparation, data collection and analysis were performed by Cheng Zeng, and Jiani Wang. Shen Zhao and Yuhan Wei assisted in data collection and statistical analysis. Cheng Zeng, Yalong Qi, Shuning Liu, Hewei Ge, and Xiaoqi Yang contributed to methodology optimization. Cheng Zeng, Yuanyi

Wang, and Yujing Tan participated in manuscript editing. The first draft of the manuscript was written by Cheng Zeng and all authors commented on previous versions of the manuscript. All authors read and approved the final manuscript. Cheng Zeng and Jiani Wang contributed equally to this work.

### Data availability

The RNA sequencing data for this study have been deposited into the Genome Sequence Archive (GSA) database under accession codes PRJCA017539 (<https://ngdc.cncb.ac.cn/bioproject/browse/PRJCA017539>). The data supporting the findings of this study are provided in the supplementary information files. Additional data are available from the corresponding author upon reasonable request.

### Ethics approval and consent to participate

All patients in the Shanghai cohort were included in the study following approval by the Ethics Committee of Fudan University Shanghai Cancer Center (FUSCC). Written informed consent was obtained from each participant prior to enrollment. The use of human tumor tissue samples was approved by the Ethics Committee of Shanghai Outdo Biotech Company (approval number: YBM-05-01, YBM-05-02).

### Competing Interests

The authors have declared that no competing interest exists.

### References

- Bray F, Laversanne M, Sung H, Ferlay J, Siegel RL, Soerjomataram I, et al. Global cancer statistics 2022: GLOBOCAN estimates of incidence and mortality worldwide for 36 cancers in 185 countries. *CA: a Cancer Journal For Clinicians*. 2024; 74: 229-63.
- Harbeck N, Penault-Llorca F, Cortes J, Gnant M, Houssami N, Poortmans P, et al. Breast cancer. *Nat Rev Dis Primers*. 2019; 5: 66.
- Waks AG, Winer EP. Breast Cancer Treatment: A Review. *JAMA*. 2019; 321: 288-300.
- Huppert LA, Gumusay O, Idossa D, Rugo HS. Systemic therapy for hormone receptor-positive/human epidermal growth factor receptor 2-negative early stage and metastatic breast cancer. *CA: a Cancer Journal For Clinicians*. 2023; 73: 480-515.
- Zeng C, Li H, Wang W, Li L, Liu B, Lan B, et al. Investigating cardiovascular diseases related to endocrine therapy in hormone receptor-positive early breast cancer: insights from a nationwide real-world study. *Cardioncology*. 2025; 11: 35.
- Finn RS, Martin M, Rugo HS, Jones S, Im S-A, Gelmon K, et al. Palbociclib and Letrozole in Advanced Breast Cancer. *The New England Journal of Medicine*. 2016; 375: 1925-36.
- Tripathy D, Im S-A, Colleoni M, Franke F, Bardia A, Harbeck N, et al. Ribociclib plus endocrine therapy for premenopausal women with hormone-receptor-positive, advanced breast cancer (MONALEESA-7): a randomised phase 3 trial. *Lancet Oncol*. 2018; 19: 904-15.
- Hortobagyi GN, Stemmer SM, Burris HA, Yap Y-S, Sonke GS, Hart L, et al. Overall Survival with Ribociclib plus Letrozole in Advanced Breast Cancer. *The New England Journal of Medicine*. 2022; 386: 942-50.
- Li Z, Zou W, Zhang J, Zhang Y, Xu Q, Li S, et al. Mechanisms of CDK4/6 Inhibitor Resistance in Luminal Breast Cancer. *Front Pharmacol*. 2020; 11: 580251.
- Vasan N, Toska E, Scaltriti M. Overview of the relevance of PI3K pathway in HR-positive breast cancer. *Ann Oncol*. 2019; 30: x3-x11.
- Dong C, Wu J, Chen Y, Nie J, Chen C. Activation of PI3K/AKT/mTOR Pathway Causes Drug Resistance in Breast Cancer. *Front Pharmacol*. 2021; 12: 628690.
- Hanker AB, Sudhan DR, Arteaga CL. Overcoming Endocrine Resistance in Breast Cancer. *Cancer Cell*. 2020; 37: 496-513.
- Wang X, Wang C, Guan J, Chen B, Xu L, Chen C. Progress of Breast Cancer basic research in China. *Int J Biol Sci*. 2021; 17: 2069-79.
- Bagchi S, Yuan R, Engleman EG. Immune Checkpoint Inhibitors for the Treatment of Cancer: Clinical Impact and Mechanisms of Response and Resistance. *Annu Rev Pathol*. 2021; 16: 223-49.
- Gaikwad S, Agrawal MY, Kaushik I, Ramachandran S, Srivastava SK. Immune checkpoint proteins: Signaling mechanisms and molecular interactions in cancer immunotherapy. *Semin Cancer Biol*. 2022; 86: 137-50.
- Harris MA, Savas P, Virassamy B, O'Malley MMR, Kay J, Mueller SN, et al. Towards targeting the breast cancer immune microenvironment. *Nature Reviews Cancer*. 2024; 24: 554-77.
- Zhang Z, Zhang Y, Liu C, Shao J, Chen Y, Zhu Y, et al. A real-world study of immune checkpoint inhibitors in advanced triple-negative breast cancer. *Cancer Innov*. 2023; 2: 172-80.
- Cardoso F, O'Shaughnessy J, Liu Z, McArthur H, Schmid P, Cortes J, et al. Pembrolizumab and chemotherapy in high-risk, early-stage, ER+/HER2- breast cancer: a randomized phase 3 trial. *Nat Med*. 2025; 31: 442-8.
- Loi S, Salgado R, Curigliano G, Romero Diaz RI, Delaloge S, Rojas Garcia CI, et al. Neoadjuvant nivolumab and chemotherapy in early estrogen receptor-positive breast cancer: a randomized phase 3 trial. *Nat Med*. 2025; 31: 433-41.
- Bian X, Liu R, Meng Y, Xing D, Xu D, Lu Z. Lipid metabolism and cancer. *J Exp Med*. 2021; 218: e20201606.
- Zeng C, Gao Y, Lan B, Wang J, Ma F. Metabolic reprogramming in cancer therapy-related cardiovascular toxicity: Mechanisms and intervention strategies. *Semin Cancer Biol*. 2025; 113: 39-58.
- Zipinotti Dos Santos D, de Souza JC, Pimenta TM, da Silva Martins B, Junior RSR, Butzene SMS, et al. The impact of lipid metabolism on breast cancer: a review about its role in tumorigenesis and immune escape. *Cell Commun Signal*. 2023; 21: 161.
- Xiao Q, Xia M, Tang W, Zhao H, Chen Y, Zhong J. The lipid metabolism remodeling: A hurdle in breast cancer therapy. *Cancer Lett*. 2024; 582: 216512.
- Wang J, Zhang W, Liu C, Wang L, Wu J, Sun C, et al. Reprogramming of Lipid Metabolism Mediates Crosstalk, Remodeling, and Intervention of Microenvironment Components in Breast Cancer. *Int J Biol Sci*. 2024; 20: 1884-904.
- Lei G, Zhuang L, Gan B. Targeting ferroptosis as a vulnerability in cancer. *Nature Reviews Cancer*. 2022; 22: 381-96.
- Li D, Li Y. The interaction between ferroptosis and lipid metabolism in cancer. *Signal Transduct Target Ther*. 2020; 5: 108.
- Lei G, Zhuang L, Gan B. The roles of ferroptosis in cancer: Tumor suppression, tumor microenvironment, and therapeutic interventions. *Cancer Cell*. 2024; 42: 513-34.
- Wang D, Wei G, Ma J, Cheng S, Jia L, Song X, et al. Identification of the prognostic value of ferroptosis-related gene signature in breast cancer patients. *BMC Cancer*. 2021; 21: 645.
- Chen Y, Zhao S, Kang Y, Zhang Y, Chang X. Identification of immune infiltration landscape on prognosis and therapy of the ferroptosis-related genes signature in breast cancer. *Biochim Biophys Acta Mol Cell Res*. 2022; 1869: 119328.
- Chang X, Xing P. Identification of a novel lipid metabolism-related gene signature within the tumour immune microenvironment for breast cancer. *Lipids Health Dis*. 2022; 21: 43.
- Shen L, Huang H, Li J, Chen W, Yao Y, Hu J, et al. Exploration of prognosis and immunometabolism landscapes in ER+ breast cancer based on a novel lipid metabolism-related signature. *Front Immunol*. 2023; 14: 1199465.
- Zeng C, Xu C, Wei Y, Ma F, Wang Y. Training and experimental validation a novel anoikis- and epithelial-mesenchymal transition-related signature for evaluating prognosis and predicting immunotherapy efficacy in gastric cancer. *J Cancer*. 2025; 16: 1078-100.
- Leek JT, Johnson WE, Parker HS, Jaffe AE, Storey JD. The sva package for removing batch effects and other unwanted variation in high-throughput experiments. *Bioinformatics*. 2012; 28: 882-3.
- Zeng C, Xu C, Liu S, Wang Y, Wei Y, Qi Y, et al. Integrated bulk and single-cell transcriptomic analysis unveiled a novel cuproptosis-related lipid metabolism gene molecular pattern and a risk index for predicting prognosis and antitumor drug sensitivity in breast cancer. *Discover Oncology*. 2025; 16: 318.
- Ritchie ME, Phipson B, Wu D, Hu Y, Law CW, Shi W, et al. limma powers differential expression analyses for RNA-sequencing and microarray studies. *Nucleic Acids Res*. 2015; 43: e47.
- Zeng C, He R, Dai Y, Lu X, Deng L, Zhu Q, et al. Identification of TGF- $\beta$  signaling-related molecular patterns, construction of a prognostic model, and prediction of immunotherapy response in gastric cancer. *Front Pharmacol*. 2022; 13: 1069204.
- Wilkerson MD, Hayes DN. ConsensusClusterPlus: a class discovery tool with confidence assessments and item tracking. *Bioinformatics*. 2010; 26: 1572-3.
- Pei S, Zhang P, Yang L, Kang Y, Chen H, Zhao S, et al. Exploring the role of sphingolipid-related genes in clinical outcomes of breast cancer. *Front Immunol*. 2023; 14: 1116839.

39. Yoshihara K, Shahmoradgoli M, Martínez E, Vegesna R, Kim H, Torres-García W, et al. Inferring tumour purity and stromal and immune cell admixture from expression data. *Nat Commun.* 2013; 4: 2612.
40. Zeng C, Liu Y, He R, Lu X, Dai Y, Qi G, et al. Identification and validation of a novel cellular senescence-related lncRNA prognostic signature for predicting immunotherapy response in stomach adenocarcinoma. *Front Genet.* 2022; 13: 935056.
41. Zeng C, Yu H, Liu X, Liu Q, Jin J. Identification and Validation of a Novel Necroptosis-Related Long Noncoding RNA Prognostic Signature for Lung Adenocarcinoma. *Biomed Res Int.* 2022; 2022: 9710540.
42. Saltz J, Gupta R, Hou L, Kurc T, Singh P, Nguyen V, et al. Spatial Organization and Molecular Correlation of Tumor-Infiltrating Lymphocytes Using Deep Learning on Pathology Images. *Cell Rep.* 2018; 23: 181-93.
43. Engebretsen S, Bohlin J. Statistical predictions with glmnet. *Clin Epigenetics.* 2019; 11: 123.
44. Chen W, Kang Y, Sheng W, Huang Q, Cheng J, Pei S, et al. A new 4-gene-based prognostic model accurately predicts breast cancer prognosis and immunotherapy response by integrating WGCNA and bioinformatics analysis. *Front Immunol.* 2024; 15: 1331841.
45. Hu H, Zou M, Hu H, Hu Z, Jiang L, Escobar D, et al. A breast cancer classification and immune landscape analysis based on cancer stem-cell-related risk panel. *NPJ Precis Oncol.* 2023; 7: 130.
46. Newman AM, Liu CL, Green MR, Gentles AJ, Feng W, Xu Y, et al. Robust enumeration of cell subsets from tissue expression profiles. *Nat Methods.* 2015; 12: 453-7.
47. Barbie DA, Tamayo P, Boehm JS, Kim SY, Moody SE, Dunn IF, et al. Systematic RNA interference reveals that oncogenic KRAS-driven cancers require TBK1. *Nature.* 2009; 462: 108-12.
48. Baird JR, Bell RB, Troesch V, Friedman D, Bambina S, Kramer G, et al. Evaluation of Explant Responses to STING Ligands: Personalized Immunosurgical Therapy for Head and Neck Squamous Cell Carcinoma. *Cancer Res.* 2018; 78: 6308-19.
49. Lin J, Lai Y, Lu F, Wang W. Targeting ACSLs to modulate ferroptosis and cancer immunity. *Trends Endocrinol Metab.* 2024; S1043-2760(24)00255-8.
50. Liu J, Tang D, Kang R. Targeting GPX4 in ferroptosis and cancer: chemical strategies and challenges. *Trends Pharmacol Sci.* 2024; 45: 666-70.
51. Jin M-Z, Jin W-L. The updated landscape of tumor microenvironment and drug repurposing. *Signal Transduct Target Ther.* 2020; 5: 166.
52. Pitt JM, Marabelle A, Eggermont A, Soria JC, Kroemer G, Zitvogel L. Targeting the tumor microenvironment: removing obstruction to anticancer immune responses and immunotherapy. *Ann Oncol.* 2016; 27: 1482-92.
53. Charoentong P, Finotello F, Angelova M, Mayer C, Efremova M, Rieder D, et al. Pan-cancer Immunogenomic Analyses Reveal Genotype-Immunophenotype Relationships and Predictors of Response to Checkpoint Blockade. *Cell Rep.* 2017; 18: 248-62.
54. Pérez-López ME, García-Gómez J, Alves MT, Paradelo A, García-Mata J, García-Caballero T. Ki-67 is a prognostic marker for hormone receptor positive tumors. *Clin Transl Oncol.* 2016; 18: 996-1002.
55. Horr C, Buechler SA. Breast Cancer Consensus Subtypes: A system for subtyping breast cancer tumors based on gene expression. *NPJ Breast Cancer.* 2021; 7: 136.
56. Pajjens ST, Vledder A, de Bruyn M, Nijman HW. Tumor-infiltrating lymphocytes in the immunotherapy era. *Cell Mol Immunol.* 2021; 18: 842-59.
57. Carey LA, Perou CM, Livasy CA, Dressler LG, Cowan D, Conway K, et al. Race, breast cancer subtypes, and survival in the Carolina Breast Cancer Study. *JAMA.* 2006; 295: 2492-502.
58. McGinn O, Ward AV, Fettig LM, Riley D, Ivie J, Paul KV, et al. Cytokeratin 5 alters  $\beta$ -catenin dynamics in breast cancer cells. *Oncogene.* 2020; 39: 2478-92.
59. Kabos P, Haughian JM, Wang X, Dye WW, Finlayson C, Elias A, et al. Cytokeratin 5 positive cells represent a steroid receptor negative and therapy resistant subpopulation in luminal breast cancers. *Breast Cancer Res Treat.* 2011; 128: 45-55.
60. Barbier O, Torra IP, Sirvent A, Claudel T, Blanquart C, Duran-Sandoval D, et al. FXR induces the UGT2B4 enzyme in hepatocytes: a potential mechanism of negative feedback control of FXR activity. *Gastroenterology.* 2003; 124: 1926-40.
61. Chen X, Wang Y-W, Gao P. SPIN1, negatively regulated by miR-148/152, enhances Adriamycin resistance via upregulating drug metabolizing enzymes and transporter in breast cancer. *J Exp Clin Cancer Res.* 2018; 37: 100.
62. Hu DG, Marri S, Hulin J-A, McKinnon RA, Mackenzie PI, Meech R. The Somatic Mutation Landscape of UDP-Glycosyltransferase (UGT) Genes in Human Cancers. *Cancers.* 2022; 14: 5708.
63. Barbier O, Duran-Sandoval D, Pineda-Torra I, Kosykh V, Fruchart J-C, Staels B. Peroxisome proliferator-activated receptor alpha induces hepatic expression of the human bile acid glucuronidating UDP-glucuronosyltransferase 2B4 enzyme. *J Biol Chem.* 2003; 278: 32852-60.
64. Dates CR, Fahmi T, Pyrek SJ, Yao-Borengasser A, Borowa-Mazgaj B, Bratton SM, et al. Human UDP-Glucuronosyltransferases: Effects of altered expression in breast and pancreatic cancer cell lines. *Cancer Biol Ther.* 2015; 16: 714-23.
65. Wang H, Dai Y, Wu X, Hu B, Wang Z, Yan M. Multiomics analysis of ferroptosis-related molecular subtypes in muscle-invasive bladder cancer immunotherapy. *Transl Cancer Res.* 2022; 11: 4089-104.
66. Frazzi R. BIRC3 and BIRC5: multi-faceted inhibitors in cancer. *Cell Biosci.* 2021; 11: 8.
67. Mendoza-Rodríguez M, Arévalo Romero H, Fuentes-Pananá EM, Ayala-Sumano J-T, Meza I. IL-1 $\beta$  induces up-regulation of BIRC3, a gene involved in chemoresistance to doxorubicin in breast cancer cells. *Cancer Lett.* 2017; 390: 39-44.
68. Feng K, He X, Qin L, Ma Z, Liu S, Jia Z, et al. Construction and validation of a ubiquitination-related prognostic risk score signature in breast cancer. *Heliyon.* 2024; 10: e35553.
69. Wu Y, Yang S, Ma J, Chen Z, Song G, Rao D, et al. Spatiotemporal Immune Landscape of Colorectal Cancer Liver Metastasis at Single-Cell Level. *Cancer Discovery.* 2022; 12: 134-53.
70. Wolfsberger J, Sakil HAM, Zhou L, van Bree N, Baldisseri E, de Souza Ferreira S, et al. TAp73 represses NF- $\kappa$ B-mediated recruitment of tumor-associated macrophages in breast cancer. *Proc Natl Acad Sci U S A.* 2021; 118: e2017089118.
71. Szpor J, Streb J, Glajcar A, Frączek P, Winiarska A, Tyrak KE, et al. Dendritic Cells Are Associated with Prognosis and Survival in Breast Cancer. *Diagnostics (Basel).* 2021; 11: 702.
72. George Warren W, Osborn M, Yates A, O'Sullivan SE. The emerging role of fatty acid binding protein 7 (FABP7) in cancers. *Drug Discov Today.* 2024; 29: 103980.
73. Lenz S, Bodnariuc I, Renaud-Young M, Butler TM, MacCallum JL. Understanding FABP7 binding to fatty acid micelles and membranes. *Biophys J.* 2023; 122: 603-15.
74. Umaru BA, Kagawa Y, Ohsaki Y, Pan Y, Chen CT, Chen DK, et al. Oleic acid-bound FABP7 drives glioma cell proliferation through regulation of nuclear lipid droplet formation. *FEBS J.* 2023; 290: 1798-821.
75. Fang X-X, Wei P, Zhao K, Sheng Z-C, Song B-L, Yin L, et al. Fatty acid-binding proteins 3, 7, and 8 bind cholesterol and facilitate its egress from lysosomes. *J Cell Biol.* 2024; 223: e202211062.
76. Cordero A, Kanojia D, Miska J, Panek WK, Xiao A, Han Y, et al. FABP7 is a key metabolic regulator in HER2+ breast cancer brain metastasis. *Oncogene.* 2019; 38: 6445-60.
77. Xie Q, Xiao Y-S, Jia S-C, Zheng J-X, Du Z-C, Chen Y-C, et al. FABP7 is a potential biomarker to predict response to neoadjuvant chemotherapy for breast cancer. *Cancer Cell Int.* 2020; 20: 562.
78. Freitas-Cortez MA, Masrourpour F, Jiang H, Mahmud I, Lu Y, Huang A, et al. Cancer cells avoid ferroptosis induced by immune cells via fatty acid binding proteins. *Mol Cancer.* 2025; 24: 40.
79. Gentles AJ, Newman AM, Liu CL, Bratman SV, Feng W, Kim D, et al. The prognostic landscape of genes and infiltrating immune cells across human cancers. *Nat Med.* 2015; 21: 938-45.
80. Chen J, Zhu Y, Wu W, Xu Y, Yang W, Ling L, et al. Association between Homologous Recombination Repair Defect Status and Long-Term Prognosis of Early HER2-Low Breast Cancer: A Retrospective Cohort Study. *Oncologist.* 2024; 29: e864-76.
81. Bassez A, Vos H, Van Dyck L, Floris G, Arijis I, Desmedt C, et al. A single-cell map of intratumoral changes during anti-PD1 treatment of patients with breast cancer. *Nat Med.* 2021; 27: 820-32.
82. Hinshaw DC, Shevde LA. The Tumor Microenvironment Innately Modulates Cancer Progression. *Cancer Res.* 2019; 79: 4557-66.